

Trends in the surface wind-wave heights in the North Indian Ocean based on 50-year NCEP/NCAR reanalysis wind-wave data

Jyoti P. Kerkar^{1,2} and Jaya Kumar Seelam^{2,3*}

¹Research Scholar, Bharathidasan University, Tiruchirappalli,
Tamil Nadu, 620024; jyoti2317@gmail.com

²CSIR-National Institute of Oceanography, Goa, 403 004, India; *jay@nio.org

³Professor, Academy of Scientific & Innovative Research, Ghaziabad, India

Abstract:

Analysis of 50 years of hourly significant wave heights of the Indian Ocean between 30°N and 60°S is carried out and linear trends of mean significant wave heights and maximum significant wave heights are obtained on annual, seasonal and decadal scales. The significant wave heights (SWH) are obtained from a third-generation spectral wind-wave model forced with six-hourly NCEP-NCAR winds over the Indian Ocean. These SWHs are validated with measurements available in the north Indian Ocean and the correlation coefficient is more than 0.87. The climatology obtained from the spectral wind wave model matches well with the climatology reported in the literature using other models and satellite-based datasets. The maximum SWH ranged from 0.25m to 22.5m with the max-SWH exceeding 7m South of 30°S, and greater than 13m between 45°S-55°S and 50°E-95°E. In the Northern Indian Ocean (NIO), max SWH reached 5.5m in the central Bay of Bengal and over 8m in the western Arabian Sea. The annual trend of the mean SWH showed an overall positive trend in the Indian Ocean, except in the west BoB, northwest Arabian Sea, and a part of the central Indian Ocean. The maximum SWH also followed an overall similar positive trend as that of mean SWH albeit with a prominent negative trend in the BoB, southeastern and northwestern Arabian Sea. There was a significant difference in the SWH trend between the seasons both spatially and temporally for all other decades. However, the maximum SWH showed highly varying trends for all the seasons and decades. The variation in the mean SWH decadal trend showed greater variation in the lower latitudes compared to the higher latitudes.

Keywords: Significant wave height, NCEP-NCAR winds, trend estimates, North Indian Ocean, decadal trends, MIKE21

Introduction:

The Indian Ocean covers approximately 20% of the water on the surface of the earth (Eakins and Sharman, 2010) and is unique as compared to the other oceans due to the monsoon wind system reversal which plays a major role in changing the wind-wave climate. As far as the variability of wind speed is concerned it is reported to be higher in the North Indian Ocean compared to the Southern Indian Ocean. However, the climatological ranges of wind speed and total significant wave height are higher in the Southern Indian Ocean. The North Indian Ocean (NIO) has a significant influence on the industrial, scientific, and engineering fields of the Indian Ocean Rim countries. The NIO plays a significant role in the rainfall of South Asia's coastal areas (Clark et al., 2000). It is vital to know the long-term variations in the wind and wave parameters while understanding the coastal environment. Only short-term wind and wave records based on in-situ measurements are available in the Indian seas (Glejin et al., 2013, Kumar, 2006, Premkumar et al., 2000, Sajiv et al., 2012). Because of the sparse measured wave data, the numerical model-derived wave data gains significant importance. Many numerical wave prediction studies for the Indian Ocean region have been carried out using Scatterometer winds (e.g., Bhatt et al., 2005, Bhatt et al., 2004, Muraleedharan et al., 2009, Swain et al., 2004, Vethamony et al., 2006) while the nearshore wave parameters for coastal regions of India have been estimated using spectral wind-wave models (e.g., Aboobacker et al., 2009). Estimation of the trends of wind waves in the NIO is the primary focus of this study. It is observed that the Arabian Sea shows high wind speed and wave conditions due to the monsoons (Kumar and Anand, 2004, Kumar and Sajiv Philip, 2010, Young, 1999). Whereas, the Bay of Bengal (BoB) is generally prone to cyclonic events which cause significant inter-annual variations in the wave parameters.

Many studies have been carried out on the wave climate variations, especially in the North Atlantic and the North Pacific regions (e.g., Allan and Komar, 2000, Caires and Swail, 2004, Carter and Draper, 1988, Gulev and Grigorieva, 2004, Soomere and Räämet, 2011, Vanem and Walker, 2013). Limited studies on wave height trends are available for regions of Persian Gulf (Vieira et al., 2020) and Red Sea (Shanas et al., 2017). Although studies on regional However, very few studies exist on the NIO (e.g., Kerkar et al., 2020, Shanas and Kumar, 2015). Wind and wave conditions are significantly impacted by climate change and climate variability. Studies indicate that wave heights have increased over the last few decades over a large area of the North Atlantic and the Norwegian Sea, with high inter-annual variability (Woolf et al., 2002). Using a 45-year ECMWF-ERA-40 reanalysis wave data and 15-year satellite altimeter records, Hemer et al. (2010) assessed the southern hemisphere's inter-annual wave climate variability. Young et al. (2011) used satellite

altimeter data over 25 years (1985-2009) to assess the significant wave height (SWH) trends in the Pacific Ocean and found that there is no statistically significant trend in the mean monthly values. However, a clear statistically significant trend of increasing wave height at high latitudes was observed but for the upper tail of the wave distribution; moreover, large neutral conditions were observed in the equatorial regions (Young et al., 2011). In the East and North Atlantic, the wave height has shown an increasing trend over the last few decades with high inter-annual variability during winter (Bacon and Carter, 1991).

Globally many studies have described wave height trends, e.g., based on voluntary observing ship data (e.g., Gulev and Grigorieva, 2004, Gulev and Grigorieva, 2006), satellite-based observations (e.g., Young, 1999, Young et al., 2011), and hindcast models based (e.g., Cox and Swail, 2001, Dobrynin et al., 2012, Wang and Swail, 2006). Future global projections which take into account the 21st century carbon emission scenarios are also studied (e.g., Hemer et al., 2013, Semedo et al., 2011). The projected changes in the annual mean wave heights are influenced by future climatic scenarios, resulting in increasing trends in the Southern Ocean and decreasing trends in the subtropics (e.g., Hemer et al., 2013, Wang et al., 2014). Long-term trends of SWH are reported globally and regionally (e.g., Semedo et al., 2011, Young et al., 2012, Young et al., 2011), while similar long-term SWH trend studies in the NIO are limited.

The projected wind-wave climate in the Indian Ocean based on the satellite observation shows an increasing trend both in wind speeds and wave heights in the North Indian Ocean and the Southern Indian Ocean (Bhaskaran et al., 2014). Satyavathi et al. (2016) showed that there is an increase in the SWH within a range of 7% to 45% along the Indian coast based on GCM model data. Gupta et al. (2015), using satellite altimeter data, analysed two transects, one for the Arabian Sea and the other for the BoB and observed an increasing trend in the past two decades. The changes in SWH and wind speed were studied using altimeter data by categorizing the Indian Ocean into six zones for the period of 17 years from 1993 to 2010 revealing an average variation of SWH, and stable wind speed (Kumar et al., 2013). Shanas and Kumar (2015) using 34 years of ERA-I reanalysis data revealed a declining trend for the annual mean and extreme wind speed and a positive trend for the 90th percentile of SWH. Anoop et al. (2015) used 34 years of ERA-I reanalysis data and showed an increasing SWH trend (>1 cm/year) in the northern NIO. Hithin et al. (2015) using satellite altimeter data showed a negative trend (2.66 cm/year) in the maximum SWH and a positive trend (0.63 cm/year) in the mean SWH at a deep-water location in the central Arabian Sea. Patra and Bhaskaran (2016) inferred that the waves in the BoB show contrasting trends, although the overall trend in the NIO is positive. It is seen that different studies within NIO showed different trends based on the

duration of the data considered. There is a need to look at these trends in comparison with a longer database and record the changes if any. The present work attempts to look at the SWH trends using 50-year hindcast SWH data generated on similar methods in the literature. The differences in the SWH trends considering various database lengths reported in the literature and the decadal variations in the SWH trends which hitherto wasn't addressed enough are the main focus of this work.

Data and Methods

A well-calibrated third-generation wind-wave model can be used to hindcast the wave climate over a longer period (e.g., Sterl et al., 1998, Wang and Swail, 2002). Owing to scanty wave measurements in the NIO, a wave hindcast database is generated and used to establish wave climate and study the SWH trends over different scales. Earlier studies on the SWH variability in NIO based on the hindcast wind wave model data use a maximum of 34 years using the ERA-1 database (e.g., Anoop et al., 2015, Shanas and Kumar, 2015). Decadal variations in the SWH trends from the limited 34-year wave data are not reported. In the present work the SWH trends (annual, decadal, seasonal) in the NIO are presented from 50 years (1971-2020) waves generated using a third-generation spectral wind-wave model MIKE-SW (DHI, 2012). The wave model results have been validated with the available measurements and the long-term trends in SWH have been assessed, which is the primary objective of this paper.

Numerical model

The third-generation spectral wind-wave model, MIKE-SW, is based on unstructured mesh and simulates the growth, transformation and dissipation of wind-generated swells and waves in the offshore and coastal areas (DHI, 2012). MIKE-SW includes the following physical phenomena a) wave growth by the action of wind, b) non-linear wave-wave interaction, c) dissipation due to white-capping, d) dissipation due to bottom friction, e) dissipation due to depth-induced wave breaking, f) refraction and shoaling due to depth variations, g) wave-current interaction, and h) effect of time-varying water depth and flooding and drying. The basic conservation equations are formulated in either Cartesian or Polar or Spherical coordinates.

The spectral-energy balance equation, which describes the development of the surface gravity wave field in space and time, forms the mathematical foundation of all numerical wave prediction models. Wave models solve this equation using different numerical methods. The energy balance equation is given (WMO, 1998) as,

$$\frac{\partial E}{\partial t} + \nabla \cdot (C_g E) = S \quad (1)$$

Where: E is the action density and is a function of $(f, \theta, x, \text{ and } t)$, f is frequency, θ is the direction of propagation, t is the time, x is space, and C_g is the deep-water group velocity. The source term ‘ S ’ expressed on the right-hand side of the equation is given by,

$$S = S_{in} + S_{nl} + S_{ds} + S_{bot} + S_{surf} \quad (2)$$

The source-sink mechanisms describe the wind input term (S_{in}), the non-linear wave-wave interaction (S_{nl}), wave energy dissipation due to white capping (S_{ds}), dissipation due to bottom friction, and dissipation due to depth-induced wave breaking (S_{surf}). The source functions S_{in} , S_{nl} , and S_{ds} are as per Komen et al. (1994). The wind input source term represents the momentum transfer by the winds to the free surface of the ocean, based on Janssen (1989, 1991). The non-linear wave-wave interaction source function is approximated by the DIA approach (Hasselmann and Hasselmann, 1985). The S_{ds} is modelled as per Hasselmann (1974) and Janssen (1989), while S_{bot} is modelled using the approach of Johnson and Kofoed-Hansen (2000). A detailed description of the wave model and various source functions is available in the MIKE SW scientific document (DHI, 2012). MIKE-SW wind-wave model has been used to simulate waves in the Indian Ocean (e.g., Kerkar et al., 2020, Patra and Bhaskaran, 2016, Remya et al., 2014). MIKE-SW is employed to assess wave climates both in the offshore and coastal areas.

Model domain and inputs

The wave model domain considered in this work covers the region between 60°S-30°N and 20°E-115°E comprising the Indian Ocean (Fig 1a). The consideration of this domain was necessary to account for the swells generated and propagating from the Southern Ocean, as the swells from the southwest or south directions strongly influence the wave climate along the west coast of India. The spatial resolution used in the coastal waters is 0.25° and for the rest of the region varied between 1° and 2°. The Earth Topography and Bathymetry version 2 (ETOPO2) data obtained from the National Geophysical Data Centre, USA, for deep water and DHI coastal mapping data (MIKE CMAP) for the coastal region were used to generate the bathymetry. The accuracy of the wave hindcast is mainly dependent on the accuracy of the input winds (Holthuijsen et al., 1996) and NCEP/NCAR reanalysis wind data (NCEP/NCAR, 2015) was used as input to the wave model. These wind data are available at six-hourly mean zonal (east-west) and meridional (north-south) surface wind components, at a resolution of 2.5°x2.5°. The NCEP/NCAR reanalysis wind consists of output from a high-resolution atmospheric model. The NCEP/NCAR model is run using observations collected from surface and upper air stations and satellite observation platforms, which

are routinely used for climate change simulations when measured wind records are not available (Mujumdar and Ghosh, 2008).

Wave height trends

SWH trends over the entire Indian Ocean are estimated to ascertain general trends of the annual mean SWH and annual maximum SWH. These trends are compared with the results available in the literature. Hourly SWH data for 50 years (1971-2020) are considered to obtain the respective mean SWH and maximum SWH for annual, decadal and seasonal (together referred to as periods). The SWH for each of these periods are subjected to least squares fit regression analysis and the slope of the least square fit line is considered as the SWH trend. Further, the Thiel-Sen non-parametric estimator (Gilbert, 1987) also known as Sen's slope, Kendall robust line-fit, single median, Kendall-Thiel robust line, etc. is also computed for the data to obtain an unbiased SWH trend for the different periods. Sen's slope trend is used to discuss the SWH trend variations in the study region. The advantage of Sen's slope is that the SWH trends are not skewed by the outliers in the data.

The annual mean SWH refers to the mean of the hourly SWH values over one year. The annual maximum SWH refers to the maximum of the hourly SWH values over one year. The decadal mean SWH refers to the mean of the hourly SWH values over one decade and similarly, the decadal maximum SWH refers to the maximum of the hourly SWH values over one decade. Similarly, the seasonal mean and maximum SWH are also computed for the three different seasons viz., southwest monsoon (June-September referred to as JJAS), northeast monsoon (October-January referred to as ONDJ) and fair-weather (February-May referred to as FMAM).

Results and discussion:

Model validation

The model results are validated by comparing the model-derived hourly SWH with *in situ* measured SWH data available in the Indian Ocean for one year. A comparison of SWH was carried out at seven locations (Fig 1b) covering both the Arabian Sea and the Bay of Bengal (BoB). The model-derived SWH compared well with the measured buoy SWH for both the Arabian Sea and the BoB locations (Table 1). The coefficient of correlation (CC) between the measured and the modelled SWH for the location AD02 in the Arabian Sea was 0.95, whereas, the RMSE was 0.64, and the bias was 0.5 for this location. Similarly, for the location BD11 in the Bay of Bengal, the CC between the measured and the modelled SWH was 0.87, RMSE was 0.4, and Bias was 0.16 (Fig 2). Overall, the model results showed a good comparison with the in situ measurements, indicating that the model-derived SWH can be used with a higher degree of confidence in the analysis.

SWH variations

The 50-year mean SWH varied from between 0.01m to 5.88m (Fig. 3). The region south of 30°S shows a remarkable increase in the mean SWH with SWH values above 3.5m with higher values (>5m) occurring in the region between 45°S-55°S and 75°E-100°E, whereas, the Northern Indian Ocean (NIO) region has a mean SWH of less than 2.5m with the annual mean SWH was less than 1.5m along the west and east coasts while it was around 2 to 2.5m near the Lakshadweep Islands and Maldives. The majority of the central Arabian Sea and central BoB showed a mean annual SWH of 2 to 2.5 m.

The 50-year maximum SWH varied between 0.25m and 22.5m (Fig 4). The region south of 30°S shows maximum SWH values above 7m with SWH values >13m occurring in the region between 45°S-55°S and 50°E-95°E. The Northern Indian Ocean (NIO) region showed a maximum SWH of about 5.5m in the central Bay of Bengal and above 8m in the western Arabian Sea. Along the west coast of India, the maximum SWH were below 4m in the northern latitudes (above 17°N) and less than 3m in the southern latitudes (between 8°N and 17°N), whereas along the east coast in the northern latitudes the mean SWH was less than 2m while in the southern latitudes.

The variation in the mean SWH and maximum SWH obtained are consistent with results reported by Naseef and Kumar (2020) wherein the strongest SWH is seen in the region 48°-52°S and 89°-93° E. Also, the higher SWH in the Arabian Sea compared to the BoB is consistent with Anoop et al (2015) where it is shown that the peak magnitude of SWH over the Arabian Sea in the western region is higher than that in the Bay of Bengal.

Decadal variations of mean SWH:

The SWH mean over each decade in comparison with the preceding decade showed that the second, third and fourth decadal mean is, in general, greater than the previous decade (i.e., first, second and third decades respectively) in the NIO, however, the fifth-decade mean is observed to be less than the fourth-decade mean (Fig 5a-d). However, the mean SWH in the central and south-central IO showed a variation that is different than NIO. The south-central IO showed that the second decadal mean is lower than the first decadal mean (Fig. 5a). Similar differences are seen along the central and northeast coast of India, the central Persian Gulf, the north-western coast of India, northern Sri Lanka and region between the African continent and Madagascar. In contrast to the difference between D1 and D2, the difference in the decadal mean SWH between D2 and D3 showed that the Persian Gulf, and the northeast region above Madagascar, showed a prominent decrease in the D3 decadal mean SWH whereas all over the IO the D3 mean was greater than D2 mean (Fig.5b). While the D3 decadal

mean SWH was in general higher than D2, the D3 mean was observed to be lower than D4 mean SWH almost all over the IO except central and northern Persian Gulf, Gulf of Aden, the northwest region above Madagascar and Somalia coast, and southeast coast of India (Fig.5c). In contrast to decadal mean SWH difference between the previous decades being on the negative which meant that the mean SWH was consistently increasing every decade till D4, the D5 mean SWH showed lower values resulting in a contrasting positive difference between D4 and D5 mean SWH all over the IO except west-southwest of Madagascar and south-central IO between 25-45 S and 40-90 E (Fig.5d).

Decadal variations of maximum SWH:

Though there was a clear indication of the overall changes in the decadal mean SWH between each of the decades, the decadal differences for the maximum SWH are not similar to the differences in the mean SWH (Fig.6a-d). The difference between maximum SWH for the first two decades D1 and D2 showed that the Arabian Sea, northeast BOB, South Andaman Sea, east African coast, Southern Ocean, and south-central IO had lower max SWH during D2 (maximum difference up to 3m) whereas the rest of the IO had higher maximum SWH (maximum difference up to 1m) (Fig. 6a). The difference between D2 and D3 more or less opposite pattern compared to D1-D2 with maximum differences being up to 3m (Fig. 6b). The D3-D4 differences in maximum SWH during D4 being less by about 3m in the eastern Arabian Sea, southeast BOB, region between Madagascar and Africa coast, most region between 5S and 10S till 75E, and along east-central IO, while remaining region of IO exhibited higher maximum SWH during D4 (Fig. 6c). The maximum SWH during D5 was higher by about 5m along the region between 10S-35S and by about 1 to 3m in majority of the IO except along the southern ocean and eastern and central BOB, and south of Indian peninsula (Fig.6d).

Annual Trends

Trends of SWH using linear regression for all of the fifty years are shown in Fig.7 for mean SWH and Fig. 9 for maximum SWH, while the trends computed using the Thiel-Sen approach (Sen's slope) are shown in Fig.8 for mean SWH and Fig. 10 for maximum SWH.

Linear annual mean SWH trends

The region below 15°S showed a positive trend in mean SWH up to 2cm/year (Fig. 7). The regions above Madagascar (12°S till 3°S; 40°E to 51°E), off north Somalia and inside the Persian Gulf showed a negative trend not exceeding -2.5mm/year. The majority of the central and eastern Arabian Sea and Bay of Bengal showed a positive trend (0 to 8mm/year). Along the west coast of India, an overall positive trend is observed (4.9mm/year) except inside the Gulf of Kachchh wherein it was a

negative trend of the order of -1.5mm/year. In the Bay of Bengal, overall it showed a positive trend with a maximum positive trend of about 6.9mm/year inside the Gulf of Mannar. However, along the east coast of India, the trends varied between -1.9 mm/year to 6.1mm/year, the negative trends being in the central and northern coastal stretches. and Eastern Arabian Sea showed negative trends up to -1.5 cm/year.

Sen's-slope based annual mean SWH trends

The region below 15°S showed a positive trend in mean SWH up to 2cm/year (Fig. 8). The regions above Madagascar and east of Madagascar (10°S till 10°N along the African coast; 11°S to 22°S in the central Indian Ocean; and between 40°E to 94°E), showed a negative trend not exceeding -2.6mm/year. The majority of the central Indian Ocean, eastern Arabian Sea and eastern Bay of Bengal showed a positive trend (0 to 6mm/year), whereas along the east coast of India, an overall negative trend is observed (-1.5mm/year). Inside the Gulf of Kachchh and Gulf of Khambhatt, negative trends were observed of the order of -0.6mm/year. Whereas, inside the Gulf of Mannar it showed a positive trend with a maximum positive trend of about 3.3mm/year.

Linear trends for annual maximum SWH

The region below 20°S showed a positive trend in maximum SWH between 9mm/year and 6cm/year (Fig. 9) except for the region bound between 37°S-41°S; and 82°E-86°E where the trend is found to be negligible. The region above 20°S to 10°S (south-central Indian Ocean) showed a negative trend not exceeding 1cm/year while the region between 10°S and 8°N (central Indian Ocean) and the majority of the central and western Arabian Sea showed a positive trend (0 to 1cm/year). Along Maharashtra, Tamil Nadu and Andhra coasts, a positive trend is observed while the rest of the Bay of Bengal and Eastern Arabian Sea showed negative trends up to -1.5 cm/year. The region below Sri Lanka 6°N and 1.5°N; 75°E-85°E showed a negative trend not exceeding -3.5 mm/year.

Sen's-slope based annual maximum SWH trends

Trends based on Sen's slope showed similar trends to the linear trend estimates in the Southern latitudes of the Indian Ocean however, the trends were between 0 and a maximum of 5-7 cm/year (Fig. 10). The south-central Indian Ocean showed a prominent negative trend not exceeding -1.5 cm/year, while the central Indian Ocean and western Arabian Sea showed positive trends of the order of 1mm/year while the central Arabian Sea showed an increased positive trend of the order of 2 cm/year. Similar to the linear trends, Sen's slope showed a predominant negative trend in the Bay of Bengal (maximum 1.8 cm/year) except along the coast up to 15°N where positive trends are seen.

The linear trends and Sen's-slope trends showed similarities in the majority of the areas. However, Sen's slope is a better value than a linear trend, further discussions are restricted to Sen's-slope trends.

Decadal variation

Mean SWH decadal trends

Decadal trends, wherein the mean SWH over each decade and the maximum SWH over each decade are estimated and compared. Although, it is understood that a change in the starting date for the first decade can bring in huge differences between each subsequent decade. For example, the decadal trend between 1971-1980 and 1975-1984 will not be the same in general. Nevertheless, in this paper five decades starting with 1971 viz., 1971-1980 (D1), 1981-1990 (D2), 1991-2000 (D3), 2001-2010 (D4) and 2011-2020 (D5) are considered for comparison.

The mean SWH trends during D1 showed a negative trend over the majority of the Indian Ocean region. However, two distinct regions in the Southern Ocean (region 1: 35°S to 50°S & 26°E to 75°E and region 2: 45°S to 50°S & 75°E to 110°E), one in the central and one in the southeast Bay of Bengal showed positive trends, two in the below bound between 26°E and to 45°S (Fig. 11a). The next decade during D2 showed an opposite trend scenario wherein the majority of the Indian Ocean showed a positive trend except western coastal stretches along the southern African coast, north-western Arabian Sea off Oman coast and Persian Gulf (Fig. 11b). The mean SWH trends during the decade of D3 showed mixed trends, the southern Indian Ocean below 25°S showed predominant positive trend except the south African coast. A negative trend is observed above in the western half of the Indian Ocean and the Andaman Sea whereas the central and eastern parts of the Indian Ocean showed a predominantly positive trend, except along the Andaman Sea, central west coast of India, central & south-eastern coast of India, and north-east coast of Sri Lanka (Fig. 11c). The fourth decade D4 showed a contrastingly positive trend in the Indian Ocean except Persian Gulf, east coast of India, central Bay of Bengal and north-east Arabian Sea (Fig. 11d). And the fifth decade D5 showed negative trend in the majority of Indian Ocean except along central African coast, eastern Indian ocean, southern Persian Gulf and mouth of Persian Gulf (Fig. 11e).

The first and last decades i.e., D1 and D5 showed predominant negative trends while the second and fourth decades showed predominantly positive trends, while the third decade showed mixed trends. This shows that in the cycle of 50 years, the trends change from positive to negative and negative to positive at decadal intervals.

Maximum SWH decadal trends

The maximum SWH trends over the decadal scale showed varying trends over different decades. The decade D1 showed a predominant negative trend in the central Indian Ocean, eastern Arabian Sea, Persian Gulf, Gulf of Aden and the major portion of the Southern Ocean. However, the eastern Indian Ocean, African and Middle East coasts and south-east of the Southern Ocean and the Bay of Bengal, exhibited positive trends (Fig. 12a). The next decade D2 showed a different trend compared to the previous decade wherein the majority of the Southern Ocean, Bay of Bengal, eastern & central Arabian Sea, Persian Gulf, Gulf of Aden and western half of the central Indian Ocean exhibited positive trends and the western Arabian Sea, eastern half of the central Indian Ocean and central African coast exhibited negative trends (Fig. 12b). The third decade D3 had a contrasting trends in comparison with the previous two decades. The majority of the western half of the central Indian Ocean including the coastal regions of the African continent, Bay of Bengal, showed negative trends while the Arabian Sea, eastern and southern parts of the central Indian Ocean showed positive trends (Fig. 12c). The subsequent decade D4 showed positive trend for the western half of the Indian Ocean, the region of roaring 40s, eastern Indian Ocean and the Bay of Bengal, whereas the north-western and south-eastern regions of Arabian Sea and central-eastern half of the Indian Ocean showed negative trends (Fig. 12d). The trends for the decade D5 showed a positive trend for the majority of the Indian ocean, and the Arabian Sea. The regions along the Oman coast, northern Persian Gulf, Gulf of Aden, east coast of India, western and south-eastern parts of the Bay of Bengal, the eastern part of the central Indian Ocean and the Southern Ocean below 50°S showed negative trends (Fig. 12e).

Comparing the first two decades, the maximum SWH trends appear to be progressing eastward. The trends that were positive in the limited western region of the Indian Ocean during D1 propagated towards the east and increased the extent of positive trends along the western region in the D2 decade. There is a reversal of trends between the D2, D3 and D4 decades wherein the positive trends became negative and vice versa in these three decades. However, such a reversal of the trends is not seen between the D4 and D5 decades.

Mean SWH trends along 55E & 90E

To further investigate the mean SWH trends over different decades, zonal variation along two meridional transects of 55E (representing western IO) and 90E (representing eastern IO) are investigated over different decades.

SWH trends along 55E:

The mean SWH trend for the 55E transect for the five-decade mean (Fig. 13a) showed alternating negative and positive values in the northern Arabian Sea till the Equator, then it followed a negative trend till 10S (-0.21cm/yr) and changed to positive trend southward with the largest positive trend being at 55S (1.39cm/yr). The first decade D1 (1971-1980) showed negative trends till 35S and thereafter showed positive trends till 45S and again showed negative trends till 55S. The second decade D2 (1981-1990) showed significantly positive trends in the overall Indian Ocean with an increasing trend towards southern latitudes (0.86 cm/yr at 25N to 7.5 cm/yr at 55S). The third decade D3 (1991-2000) showed negative trends till 20S (0.27 to 2 cm/yr) and showed positive increasing trends (0.24 cm/yr at 25S to 6.2 cm/yr at 45S) and further reduced to 2.8 cm/yr at 55S. The fourth decade D4 (2001-2010) showed increasing positive trends till 30S (1.03 cm/yr at 15N to 4.14 cm/yr at 35S) and further showed decreasingly positive trends till 55S (2.4 cm/yr; 1.8 cm/yr at 50S). The fifth decade D5 (2011-2020) showed negative trends all over the region except around 55S (0.74 cm/yr). During this D5 decade, the negative trends increased southwards between 25N (-0.21 cm/yr) and 15N (-1.3 cm/yr) and at the equator the trend value was negligible and further increased negatively till 45S (-2.9 cm/yr) and changed the direction to positive trend at 55S (0.74 cm/yr).

Along the 55E transect, the mean SWH trends in the northern Arabian Sea (25N) for all decades as well as for the mean showed a negative trend of the order of 0.21 to 0.48 cm/s, while the largest variation was between -2.9cm/s and 6.4cm/s was seen at 50S. The region of 45S is found to be a region beyond which the trends change rapidly in opposite directions for the first, third and fifth decades, whereas for the fourth decade, the turning point for the reversal of the trend was 35S and for the second decade there was no reversal of trends.

SWH trends along 90E:

The mean SWH trend for the 90E transect (Fig. 13b) for the five-decade mean showed positive values in the BoB till 5S (0.04 cm/yr), then it followed a negative trend till 20S (-0.08 cm/yr) and changed to positive trend southward with the largest positive trend being at 55S (1.65 cm/yr). The first decade D1 (1971-1980) showed negative trends from 25N (-1.02 cm/yr) till the equator (-0.2 cm/yr) and thereafter showed slight positive trends till 10S (0.26 cm/yr) and again showed negative trends till 20S (-2.48 cm/yr), thereafter showed increasing positive trends till 55S (4.76 cm/yr). The second decade D2 (1981-1990) showed significantly positive trends in the overall Indian Ocean with an increasing trend towards southern latitudes (0.58 cm/yr at 15N to 5.9 cm/yr at 55S). The third decade D3 (1991-2000) showed a decreasing trend from 20N (0.53 cm/yr) to 10N (-0.23 cm/yr) and then an increasingly positive trend from 10N to 40S (2.78 cm/yr), further showed a reversing trend till 45S (0.08 cm/yr) before showing positively increasing trends till 55S (7.7 cm/yr). The fourth

decade D4 (2001-2010) followed a similar trend as that of D3, wherein alternating increase and decrease in trend is seen till 15S. However, from 15S to 35S increasing trend and a decreasing trend till 45S and a further increasing trend till 55S (6.47 cm/yr). The fifth decade D5 (2011-2020) showed negative trends all over the region with maximum negative trends varying between -1.18 cm/yr (55S) and -3.6 cm/yr (35S), while the region between 30S and 20N showed a negative trend between -2.2 cm/yr and -1.2 cm/yr.

Along the 90E transect, the mean SWH trends in the BoB (25N) for all decades as well as for the five-decade mean varied between -1.97 cm/yr to 2.57 cm/s, while the largest variation was between -1.18 cm/s and 7.72 cm/s was seen at 55S. The region between the 40S and 45S is found to be a region beyond which the trends change rapidly in opposite directions for the first, third and fourth decades, whereas for the fifth decade, the turning point for the reversal of the trend was 35S and for the second decade there was no reversal of trends.

The satellite altimeter-based daily maximum SWH data shown by Gupta et al. (2015), wherein two transects, one for the AS and the other for the BoB showed (i) an increasing trend in the two decades (1992-2012) and (ii) a pronounced increase in the SO basin especially between 45S and 55S. The studies of Gupta et al (2015) support the present study results which also show that the SWH trends between the decades D2 and D3 showed an increasing trend in the northern latitudes as well as pronounced variation in the SWH trend in the southern latitudes (Fig. 13a and Fig 13b).

Seasonal Trends

Seasonal wave heights are used to analyse the temporal variability. The NIO is largely seasonal with energetic waves during June-September and relatively calm conditions during the rest of the year. Trend analysis for SWH for different seasons is carried out considering three seasons, viz., (1) Pre-monsoon [FMAM: February-May], (2) Monsoon [JJAS: June-September] and (3) Post-monsoon [ONDJ: October-January]. The trends of SWH (mean and maximum) for each of the three seasons and each of the five decades are inter-compared. Further, the trends between the seasons within each decade are also discussed.

Seasonal trends of mean SWH

FMAM: During the first decade D1 (Fig. 14a), the southern Indian Ocean below 25S, the eastern Indian Ocean including central and southern BoB and the region adjoining Madagascar showed positive trends for mean Hs, while negative trends were observed in the majority of the Arabian Sea, the region between 15S and 25S, along the African coastal waters and northernmost regions of BoB. During the second decade D2 (Fig. 14b), there was a positive trend in the entirety of the Indian

Ocean except for a small region in the westernmost Persian Gulf and along the African coast west of Madagascar. During the third decade D3 (Fig. 14c), the majority of the Indian Ocean showed a positive trend while the regions between 15S and 45S showed patches of alternating negative trends. The decade four D4 (Fig. 14d) showed a positive trend over the entire Indian Ocean except in the Persian Gulf and interior region of the Gulf of Aden. Whereas during the fifth decade D5 (Fig. 14e), the majority of the Indian Ocean showed a negative trend except the region between 25S and 45S in the south-eastern Indian Ocean, the region below 40S in the South-western Indian Ocean, alternating patches in the central Indian Ocean and small parts of Arabian Sea.

JJAS: The majority of the Indian Ocean showed negative trends during D1 (Fig. 14f). However, the south-eastern region of the Southern Ocean, region bounded by 45S-30S and 35E-60E, eastern BoB and southeast coast of India, south of the equatorial Indian Ocean between 0-15S and 80-100E, and small parts of south-western Arabian Sea and the region between Madagascar and African coast showed positive trends. During D2 (Fig. 14g), the majority of the Indian Ocean showed positive trends. However, the Bob, Arabian Sea, region between Madagascar and the African coast and south of the African coast showed negative trends. During D3 (Fig. 14h), a major portion of the western Indian Ocean including the Arabian Sea, Persian Gulf, and central and eastern BoB showed negative trends while the eastern half of the Indian Ocean, Gulf of Aden, and north-eastern BoB showed positive trends. During D4 (Fig. 14i) the majority of the Indian Ocean showed a positive trend except for small regions in the southern Indian Ocean (40S-50S & 45E-80E; 15S-20S & 85E-110E), southwest BoB and south-eastern coast of India. During D5 (Fig. 14j), the majority of the Indian Ocean showed negative trends. The following regions showed positive trends: The Persian Gulf, the western region of the Equatorial Indian Ocean, the central Indian Ocean and the Southern Ocean.

ONDJ: During D1, most of the region south of 5S, the region between Oman and northwest India and along the southeast coast of India showed a positive trend. Most of the Arabian Sea, BoB, east central IOB and region between the 40S and 55S showed negative trends (Fig. 14k). During D2 (Fig. 14l), the eastern half of the Indian Ocean including BoB, the western Indian Ocean along the African and UAE coast, and the Southern Ocean south of 42S showed positive trend while the Eastern and northwest Arabian Sea, southcentral IO southern African coast showed negative trends. The majority of the Indian Ocean exhibited positive trends during D3 (Fig. 14m) while patches along the 40S, 15S, northwest region between Madagascar and the African coast, Persian Gulf and Gulf of Aden showed negative trends. During D4 (Fig. 14n), the entire Indian Ocean showed a positive trend except for small regions of the Gulf of Aden, the central Persian Gulf and the region between 45S-50S and 70E-75E. During D5 (Fig. 14o), almost the opposite of Decade 2 is observed wherein the

eastern half of the IO, coastal Africa, and northeast Arabian Sea exhibited negative trends while the western half of IO, south-western Southern Ocean showed positive trends.

Seasonal trends of maximum SWH

The trends of maximum SWH for different seasons showed varied likeness with that of the mean Hs. Some decades showed similar trends and for some decades it showed a different trend.

FMAM:

During D1 (Fig. 15a), negative trends were seen predominantly in the Arabian Sea including the Gulf of Aden, the eastern half of BOB, a major portion of the eastern half of the Indian Ocean below 15S and the south-western part of the Southern Ocean, South of Madagascar. Positive trends are seen in the western Bay of Bengal, the central Indian Ocean below 10N, the south-eastern region of the Southern Ocean and the Persian Gulf. However, positive trends are seen in the entirety of the Indian Ocean with small regions around Madagascar and the eastern part of the central Indian Ocean during D2 (Fig. 15b). During D3 (Fig. 15c), the majority of the western Indian Ocean between 10N and 45S showed negative trends while the eastern half of the Indian Ocean, Arabian Sea and BoB and southern region of Southern Ocean showed positive trends. Whereas, during D4 (Fig. 15d), positive trends are seen in the BoB, Arabian Sea, and the whole of the Indian Ocean except the southeastern part between 30S and 50S. The eastern region of the Andaman Sea, Persian Gulf and Gulf of Aden, central Arabian Sea and northwest region of Madagascar showed negative trends. During D5, the region along the African coast, south-eastern Southern Ocean, eastern Andaman Sea, east coast of India, interior regions of the Gulf of Aden and Persian Gulf showed negative trends while a majority of the central, eastern and south-western Indian Ocean showed positive trends (Fig. 15e).

JJAS: During D1 (Fig. 15f), the region along the African coast, south-eastern Southern Ocean, eastern Andaman Sea, BoB, interior regions of the Persian Gulf, south-western Arabian Sea, and eastern part of central Indian Ocean showed positive trends while a majority of the Indian Ocean, eastern Arabian Sea and Gulf of Aden showed negative trends. During D2 (Fig. 15g), positive trends were seen in the Persian Gulf, Gulf of Aden, eastern-central and south-western Arabian Sea, eastern and central BoB, central IO below the equator up to 15S and Southern Ocean (below 35S in the western region and 50S in the eastern region). Negative trends were seen in a majority of the central (15S to 45S) and eastern IO, western Arabian Sea, eastern BoB, Andaman Sea and south-western Southern Ocean. During D3 (Fig. 15h), contrasting trends were seen in the Arabian Sea and BoB, while BoB showed negative trends, Arabian Sea exhibited positive trends. The western half of the central IO and the region below 45S between 50E and 100E showed negative trends whereas the

majority of the central, eastern and western IO showed positive trends. In contrast to D3, during D4 (Fig. 15i) the western half of the IO, and the south-eastern part of the Southern Ocean, BoB, central and western Arabian Sea showed positive trends while the eastern half of the IO barring the Southern Ocean showed negative trends. During D5 (Fig. 15j), the western Arabian Sea, western BoB, Andaman Sea, the southwest region along Africa, the Southern Ocean region below the 50S, and central-eastern IO showed negative trends while the Arabian Sea, central western IO and the region between and 55S on the eastern IO showed positive trends.

ONDJ: Positive trends were seen during D1 (Fig. 15k) in the Southern Ocean region below the 50S, central IO between the equator and 15S, the southern region below India and Sri Lanka, south-eastern BoB and south central IO. The remaining region comprising of majority of the western Indian Ocean, south central Indian Ocean, Arabian Sea, and central and eastern BoB showed negative trends. During D2 (Fig. 15l), the majority of the region comprising the central Indian Ocean, south-eastern BoB and Arabian Sea showed negative trends. A major portion of the Southern Ocean, east-central IO and region around Madagascar showed positive trends. The trends in D3 were similar to the D2 for a major portion of the IO below the equator. However, in the northern IO, Arabian Sea (western and central) and eastern BoB showed positive trends while central and western BoB showed negative trends (Fig. 15m). During D4 (Fig. 15n) majority of the study region showed positive trends except for small portion in the southern regions below 35S, Persian Gulf and Gulf of Aden which showed negative trends. During D5 (Fig. 15o), the Arabian Sea (excluding the central region), the western IO (excluding the region along the African coast between central Somalia and Mozambique), and northern BoB showed a positive trend. While the eastern half of IO, BoB, and region along the African coast showed a negative trend.

Caires and Swail (2004) analysed the global mean SWH trends, seasonal SWH trends and extreme SWH trends for 40 years (1958-2001) of reanalysis data. Their results were restricted to trend values greater than or less than 1 cm/year for all the SWH considered (i.e., mean, 90th percentile and 99th percentile). There is not much of a variation seen in the Indian Ocean except a negative trend in the eastern Arabian Sea during July-August-September and a predominant positive trend in the Southern Ocean for all of the seasons. The present work showcases trend variation for values less than 1 cm/year and therefore the subtle variations in the trends over the Indian Ocean can be seen in detail, similar to the recent results of Sreelakshmi and Bhaskaran (2020) who used the ERA-5 dataset for 45 years.

Conclusions:

The mean SWH ranged from 0.01m to 5.88m. South of 30°S, the mean SWH surged, surpassing 3.5m, and peaking (>5m) from 45°S-55°S and 75°E-100°E. The Northern Indian Ocean (NIO), including the Central Arabian Sea and Central Bay of Bengal both displayed a mean annual SWH of 2 to 2.5m, while along the coasts the SWH dropped to less than 1.5m. Whereas, the maximum SWH ranged from 0.25m to 22.5m. South of 30°S, max SWH exceeded 7m, with peaks >13m between 45°S-55°S and 50°E-95°E. In the Northern Indian Ocean (NIO), max SWH reached 5.5m in the central Bay of Bengal and over 8m in the western Arabian Sea. The SWH climatology findings align with Naseef and Kumar (2020), highlighting the strongest SWH in the 48°-52°S and 89°-93°E regions. Similarly, the Arabian Sea exhibited higher SWH compared to the Bay of Bengal, particularly in the western Arabian Sea, as noted by Anoop et al (2015).

The annual trend of the mean SWH showed an overall positive trend in the Indian Ocean, except in the west BoB, northwest Arabian Sea, and a part of the central Indian Ocean. The maximum SWH also followed an overall similar positive trend as that of mean SWH albeit with a prominent negative trend in the BoB, southeastern and northwestern Arabian Sea. The decadal mean SWH over the decades generally increased in the North Indian Ocean (NIO), with the second (D2), third (D3), and fourth (D4) decades surpassing their respective preceding decades. However, the fifth decade (D5) saw a decrease compared to the fourth. In the Central and South Central Indian Ocean, the pattern differed wherein the second decade had a lower mean than the first. Contrary to the difference between D1 and D2, the D2 to D3 mean SWH showed a notable decrease in the Persian Gulf and the northeast region above Madagascar. Across the IO, the D3 mean SWH was generally higher than the D2 mean. While the D3 mean SWH was higher overall than D2, it was lower than the D4 mean SWH except in the western IO, and southeast coast of India. However, in contrast to previous decades, where mean SWH consistently increased, the D5 mean SWH showed lower values throughout the IO, except for a smaller region in the west-southwest of Madagascar and south-central IO between 25-45 S and 40-90 E. The variations in the mean SWH decadal trends showed an alternating positive and negative trend at decadal intervals starting from D1 (1971-1980). Whereas, the maximum SWH decadal trends between D2 to D4 showed alternating decadal trends but the last decade D5 did not show a reversal in comparison with D4.

The variation in the mean SWH decadal trend showed greater variation in the lower latitudes compared to the higher latitudes. The seasonal trends of mean SWH showed that the fourth decade showed an overall positive trend for the majority of the region for all three different seasons considered. Apart from the second and fourth decades for the FMAM season being similar, there

was a significant difference in the SWH trend between the seasons both spatially and temporally for all other decades. However, the maximum SWH showed highly varying trends for all the seasons and decades.

Acknowledgements:

Authors thank their respective Institutes for the support and facilities provided. First Author acknowledges the financial support from the Department of Science and Technology, Govt. of India through the Women Scientist Scheme (WOS-A). The Indian National Centre for Ocean Information Services (INCOIS), Ministry of Earth Sciences, India, is acknowledged for the buoy data used in the model validation. This manuscript is a part of the doctoral thesis of the first author registered with Bharathidasan University, Tiruchirappalli. NIO contribution number is XXXX (will be provided after the manuscript is accepted).

Conflict of interest: There is no conflict of interest.

Funding: CSIR – NIO contributed a majority of the funding for salaries and equipment. Part funding provided by the Ministry of Science and Technology through the Women Scientist Scheme for the First Author.

Author's contribution statement: JKS conceptualized the work, contributed to model setup and data analysis, and in manuscript editing and finalizing. JPK carried out the numerical modelling, data analysis and prepared the manuscript.

References:

- ABOBACKER, V. M., VETHAMONY, P., SUDHEESH, K. & RUPALI, S. P. 2009. Spectral characteristics of the nearshore waves off Paradip, India during monsoon and extreme events. *Natural Hazards*, 49, 311-323.
- ALLAN, J. & KOMAR, P. 2000. Are ocean wave heights increasing in the eastern North Pacific? *Eos, Transactions American Geophysical Union*, 81, 561-567.
- ANOOP, T. R., KUMAR, V. S., SHANAS, P. R. & JOHNSON, G. 2015. Surface Wave Climatology and Its Variability in the North Indian Ocean Based on ERA-Interim Reanalysis. *Journal of Atmospheric and Oceanic Technology*, 32, 1372-1385.
- BACON, S. & CARTER, D. J. T. 1991. Wave climate changes in the North Atlantic and North Sea. *International Journal of Climatology*, 11, 545-558.
- BHASKARAN, P. K., GUPTA, N. & DASH, M. K. 2014. Wind-wave Climate Projections for the Indian Ocean from Satellite Observations. *J Marine Sci Res Development*.

- BHATT, V., KUMAR, R., BASU, S. & AGARWAL, V. K. 2005. Assimilation of altimeter significant wave height into a third-generation global spectral wave model. *IEEE Transactions on Geoscience and Remote Sensing*, 43, 110-117.
- BHATT, V., SARKAR, A., KUMAR, R., BASU, S. & AGARWAL, V. K. 2004. Impact of Oceansat-I MSMR data on analyzed oceanic winds and wave predictions. *Ocean Engineering*, 31, 2283-2294.
- CAIRES, S. & SWAIL, V. 2004. Global wave climate trend and variability analysis. In: COSPONSORS, U. A. E. R. A. D. C. S. C. A. H. L. A. (ed.) *8th Int. Workshop on Wave Hindcasting and Forecasting*. Oahu, Hawaii.
- CARTER, D. J. T. & DRAPER, L. 1988. Has the north-east Atlantic become rougher? *Nature*, 332, 494-494.
- CLARK, C. O., COLE, J. E. & WEBSTER, P. J. 2000. Indian Ocean SST and Indian Summer Rainfall: Predictive Relationships and Their Decadal Variability. *Journal of Climate*, 13, 2503-2519.
- COX, A. T. & SWAIL, V. R. 2001. A global wave hindcast over the period 1958–1997: Validation and climate assessment. *Journal of Geophysical Research: Oceans*, 106, 2313-2329.
- DHI 2012. Scientific Documentation, Mike21 SW module. Horsholm, Denmark: DHI water and environment.
- DOBRYNIN, M., MURAWSKY, J. & YANG, S. 2012. Evolution of the global wind wave climate in CMIP5 experiments. *Geophysical Research Letters*, 39.
- EAKINS, B. W. & SHARMAN, G. F. 2010. *Volumes of the World's Oceans from ETOPO1* [Online]. Boulder, CO: NOAA National Geophysical Data Center. Available: https://www.ngdc.noaa.gov/mgg/global/etopo1_ocean_volumes.html [Accessed 9/9/2020 2020].
- GILBERT, R. O. 1987. *Statistical Methods for Environmental Pollution Monitoring*. John Wiley and Sons.
- GLEJIN, J., SANIL KUMAR, V., BALAKRISHNAN NAIR, T. M. & SINGH, J. 2013. Influence of winds on temporally varying short and long period gravity waves in the near shore regions of the eastern Arabian Sea. *Ocean Science*, 9, 343-353.
- GULEV, S. K. & GRIGORIEVA, V. 2004. Last century changes in ocean wind wave height from global visual wave data. *Geophysical Research Letters*, 31.
- GULEV, S. K. & GRIGORIEVA, V. 2006. Variability of the Winter Wind Waves and Swell in the North Atlantic and North Pacific as Revealed by the Voluntary Observing Ship Data. *Journal of Climate*, 19, 5667-5685.
- GUPTA, N., BHASKARAN, P. K. & DASH, M. K. Recent trends in wind-wave climate for the Indian Ocean. 2015.
- HASSELMANN, K. 1974. On the spectral dissipation of ocean waves due to white capping. *Boundary-Layer Meteorology*, 6, 107-127.

- HASSELMANN, S. & HASSELMANN, K. 1985. Computations and Parameterizations of the Nonlinear Energy Transfer in a Gravity-Wave Spectrum. Part I: A New Method for Efficient Computations of the Exact Nonlinear Transfer Integral. *Journal of Physical Oceanography*, 15, 1369-1377.
- HEMER, M. A., CHURCH, J. A. & HUNTER, J. R. 2010. Variability and trends in the directional wave climate of the Southern Hemisphere. *International Journal of Climatology*, 30, 475-491.
- HEMER, M. A., FAN, Y., MORI, N., SEMEDO, A. & WANG, X. L. 2013. Projected changes in wave climate from a multi-model ensemble. *Nature Climate Change*, 3, 471-476.
- HITHIN, N. K., KUMAR, V. S. & SHANAS, P. R. 2015. Trends of wave height and period in the Central Arabian Sea from 1996 to 2012: A study based on satellite altimeter data. *Ocean Engineering*, 108, 416-425.
- HOLTHUIJSEN, L. H., BOOIJ, N. & BERTOTTI, L. 1996. The Propagation of Wind Errors Through Ocean Wave Hindcasts. *Journal of Offshore Mechanics and Arctic Engineering*, 118, 184-189.
- JANSSEN, P. A. E. M. 1989. Wave-Induced Stress and the Drag of Air Flow over Sea Waves. *Journal of Physical Oceanography*, 19, 745-754.
- JANSSEN, P. A. E. M. 1991. Quasi-linear Theory of Wind-Wave Generation Applied to Wave Forecasting. *Journal of Physical Oceanography*, 21, 1631-1642.
- JOHNSON, H. K. & KOFOED-HANSEN, H. 2000. Influence of Bottom Friction on Sea Surface Roughness and Its Impact on Shallow Water Wind Wave Modeling. *Journal of Physical Oceanography*, 30, 1743-1756.
- KERKAR, J. P., SEELAM, J. K. & JENA, B. K. 2020. Wave Height Trends off Central West Coast of India. *Journal of Coastal Research*, 89, 97-104, 8.
- KOMEN, G. J., CAVALERI, L., DONELAN, M., HASSELMANN, K., HASSELMANN, S. & JANSSEN, P. A. E. M. 1994. *Dynamics and Modelling of Ocean Waves*, Cambridge, Cambridge University Press.
- KUMAR, E. D., SANNASIRAJ, S. A., SUNDAR, V. & POLNIKOV, V. G. 2013. Wind-Wave Characteristics and Climate Variability in the Indian Ocean Region Using Altimeter Data. *Marine Geodesy*, 36, 303-318.
- KUMAR, V. S. 2006. Variation of wave directional spread parameters along the Indian coast. *Applied Ocean Research*, 28, 93-102.
- KUMAR, V. S. & ANAND, N. M. 2004. Variations in wave direction estimated using first and second order Fourier coefficients. *Ocean Engineering*, 31, 2105-2119.
- KUMAR, V. S. & SAJIV PHILIP, C. 2010. Variations in long term wind speed during different decades in Arabian Sea and Bay of Bengal. *Journal of Earth System Science*, 119, 639-653.

- MUHAMMED NASEEF, T. & SANIL KUMAR, V. 2020. Climatology and trends of the Indian Ocean surface waves based on 39-year long ERA5 reanalysis data. *International Journal of Climatology*, 40, 979-1006.
- MUJUMDAR, P. P. & GHOSH, S. 2008. Climate change impact on hydrology and water resources. *ISH Journal of Hydraulic Engineering*, 14, 1-17.
- MURALEEDHARAN, G., SINHA, M., RAO, A. D., NAIR, N. U. & KURUP, P. G. 2009. Estimation of wave period statistics using numerical coastal wave model. *Natural Hazards*, 49, 165-186.
- NCEP/NCAR. 2015. *The NCEP/NCAR Reanalysis Project* [Online]. Earth System Research Laboratory, Boulder, CO, USA. Available: <https://www.esrl.noaa.gov/psd/data/reanalysis/reanalysis.shtml> [Accessed 13 January 2015].
- PATRA, A. & BHASKARAN, P. K. 2016. Trends in wind-wave climate over the head Bay of Bengal region. *International Journal of Climatology*, 36, 4222-4240.
- PREMKUMAR, K., RAVICHANDRAN, M., KALSI, S. R., SENGUPTA, D. & GADGIL, S. 2000. First results from a new observational system over the Indian seas. *Current Science*, 78, 323-330.
- REMYA, P. G., KUMAR, R. & BASU, S. 2014. An assessment of wind forcing impact on a spectral wave model for the Indian Ocean. *Journal of Earth System Science*, 123, 1075-1087.
- SAJIV, P. C., SANIL KUMAR, V., GLEJIN, J., DORA, G. U. & VINAYARAJ, P. 2012. Interannual and seasonal variations in nearshore wave characteristics off Honavar, west coast of India. *Current Science*, 103, 286-292.
- SATYAVATHI, P., DEO, M. C., KERKAR, J. & VETHAMONY, P. 2016. Reevaluation of Design Waves Off the Western Indian Coast Considering Climate Change. *Marine Technology Society Journal*, 50, 88-98.
- SEMEDO, A., SUŠELJ, K., RUTGERSSON, A. & STERL, A. 2011. A Global View on the Wind Sea and Swell Climate and Variability from ERA-40. *Journal of Climate*, 24, 1461-1479.
- SHANAS, P. R., ABOOBACKER, V. M., ALBARAKATI, A. M. A. & ZUBIER, K. M. 2017. Climate driven variability of wind-waves in the Red Sea. *Ocean Modelling*, 119.
- SHANAS, P. R. & KUMAR, V. S. 2015. Trends in surface wind speed and significant wave height as revealed by ERA-Interim wind wave hindcast in the Central Bay of Bengal. *International Journal of Climatology*, 35, 2654-2663.
- SOOMERE, T. & RÄÄMET, A. 2011. Long-term spatial variations in the Baltic Sea wave fields. *Ocean Sci.*, 7, 141-150.
- SREELAKSHMI, S. & BHASKARAN, P. K. 2020. Wind-generated wave climate variability in the Indian Ocean using ERA-5 dataset. *Ocean Engineering*, 209, 107486.

- STERL, A., KOMEN, G. J. & COTTON, P. D. 1998. Fifteen years of global wave hindcasts using winds from the European Centre for Medium-Range Weather Forecasts reanalysis: Validating the reanalyzed winds and assessing the wave climate. *Journal of Geophysical Research: Oceans*, 103, 5477-5492.
- SWAIN, J., PRASADA RAO, C. V. K. & VENKITACHALAM, N. R. 2004. Performance evaluation of third-generation wave model for the Indian Ocean region using analysed winds. *METOC*.
- VANEM, E. & WALKER, S.-E. 2013. Identifying trends in the ocean wave climate by time series analyses of significant wave height data. *Ocean Engineering*, 61, 148-160.
- VETHAMONY, P., SUDHEESH, K., RUPALI, S. P., BABU, M. T., JAYAKUMAR, S., SARAN, A. K., BASU, S. K., KUMAR, R. & SARKAR, A. 2006. Wave modelling for the north Indian Ocean using MSMR analysed winds. *International Journal of Remote Sensing*, 27, 3767-3780.
- VIEIRA, F., CAVALCANTE, G. & CAMPOS, E. 2020. Analysis of wave climate and trends in a semi-enclosed basin (Persian Gulf) using a validated SWAN model. *Ocean Engineering*, 196, 106821.
- WANG, X. L., FENG, Y. & SWAIL, V. R. 2014. Changes in global ocean wave heights as projected using multimodel CMIP5 simulations. *Geophysical Research Letters*, 41, 1026-1034.
- WANG, X. L. & SWAIL, V. R. 2002. Trends of Atlantic Wave Extremes as Simulated in a 40-Yr Wave Hindcast Using Kinematically Reanalyzed Wind Fields. *Journal of Climate*, 15, 1020-1035.
- WANG, X. L. & SWAIL, V. R. 2006. Climate change signal and uncertainty in projections of ocean wave heights. *Climate Dynamics*, 26, 109-126.
- WMO 1998. Guide to Wave Analysis and Forecasting. World Meteorological Organization.
- WOOLF, D. K., CHALLENGER, P. G. & COTTON, P. D. 2002. Variability and predictability of the North Atlantic wave climate. *Journal of Geophysical Research: Oceans*, 107, 9-1-9-14.
- YOUNG, I. R. 1999. Seasonal variability of the global ocean wind and wave climate. *International Journal of Climatology*, 19, 931-950.
- YOUNG, I. R., VINOTH, J., ZIEGER, S. & BABANIN, A. V. 2012. Investigation of trends in extreme value wave height and wind speed. *Journal of Geophysical Research: Oceans*, 117.
- YOUNG, I. R., ZIEGER, S. & BABANIN, A. V. 2011. Global Trends in Wind Speed and Wave Height. *Science*, 332, 451-455.

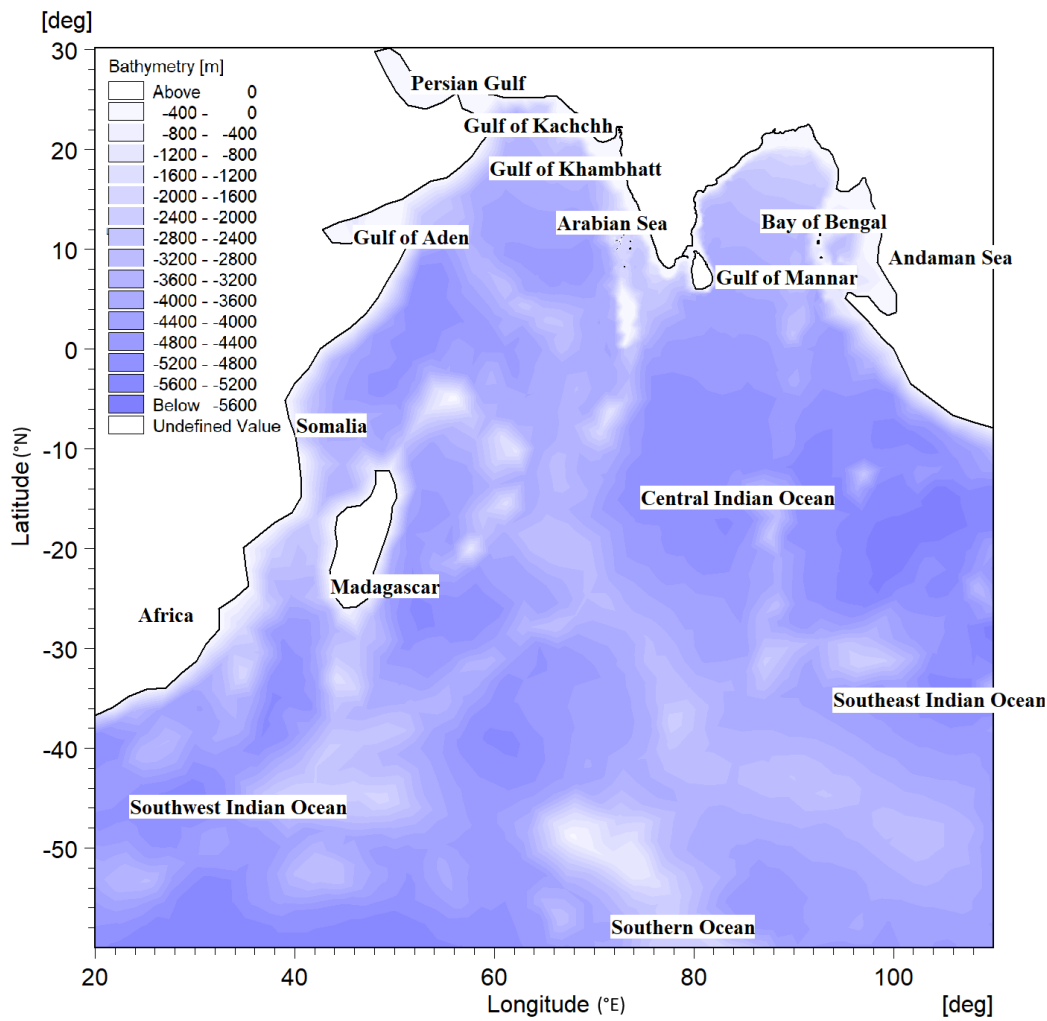
Table Captions

Table 1: Error statistics estimated between the measured and the modelled SWH in the Indian Ocean

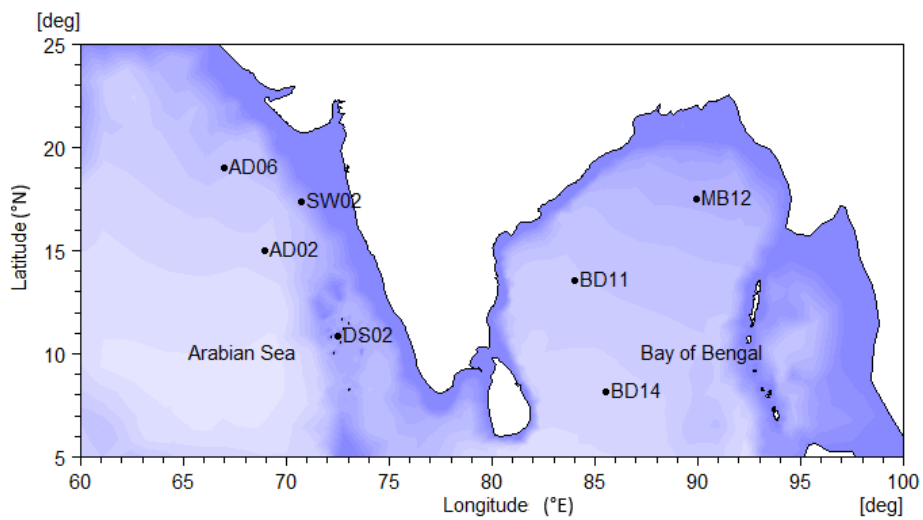
Location	Latitude (°N)	Longitude (°E)	Bias	RMSE	Scatter Index	Correlation Coefficient
AD02	15.01	68.98	0.50	0.64	0.33	0.95
AD06	19.00	66.97	0.49	0.63	0.37	0.94
BD11	13.54	84.02	0.16	0.40	0.25	0.87
BD14	8.16	85.54	0.4	0.52	0.27	0.87
DS02	10.84	72.51	0.6	0.68	0.54	0.88
MB12	17.49	89.92	0.56	0.62	0.52	0.90
SW02	17.36	70.70	0.34	0.57	0.35	0.95

Figure Captions

- Fig. 1. (a) Location map showing study region and model domain (showing different regions: BOB, Gulf of Mannar, Arabian Sea, Gulf of Kachchh, Gulf of Khambhatt, Andaman Sea, Persian Gulf, Gulf of Aden, central IO, southeast IO, southwest IO, Southern Ocean, Madagascar, Somalia, Africa), (b) locations of wave buoys used in model validation
- Fig. 2. Comparison plots of measured (y-axis) and modelled (x-axis) SWH for different locations in the north Indian Ocean. See text and table for details of locations and the correlation coefficients
- Fig. 3. Comparison plots of measured (y-axis) and modelled (x-axis) SWH for different locations in the north Indian Ocean. See text and table for details of locations and the correlation coefficients
- Fig. 4. Maximum SWH over the 50 years
- Fig. 5. Difference between the mean SWH of decades (a) D1 and D2 (b) D2 and D3 (c) D3 and D4 and (d) D4 and D5
- Fig. 6. Difference between the maximum SWH of decades (a) D1 and D2 (b) D2 and D3 (c) D3 and D4 and (d) D4 and D5
- Fig. 7. Trends of Mean SWH for 50 years using linear regression
- Fig. 8. Trends of Mean SWH for 50 years using Thiell-Sen's slope approach
- Fig. 9. Linear trends for maximum SWH for 50 years
- Fig. 10. Sen's slope trends for maximum SWH for 50 years
- Fig. 11. Trends of mean SWH for (a) decade D1, (b) decade D2, (c) decade D3, (d) decade D4 and (e) decade D5
- Fig. 12. Trends of maximum SWH for (a) decade D1, (b) decade D2, (c) decade D3, (d) decade D4 and (e) decade D5
- Fig. 13. Mean SWH trends along (a) 55E, (b) 90E
- Fig. 14. Seasonal mean SWH trend SWH trend for different decades and different seasons
- Fig. 15. Seasonal maximum SWH trend for different decades and different seasons



(a)



(b)

Fig. 1. Location map showing study region and model domain (showing different regions: BOB, Gulf of Mannar, Arabian Sea, Gulf of Kachchh, Gulf of Khambhatt, Andaman Sea, Persian Gulf, Gulf of Aden, central IO, southeast IO, southwest IO, Southern Ocean, Madagascar, Somalia, Africa), (b) locations of wave buoys used in model validation

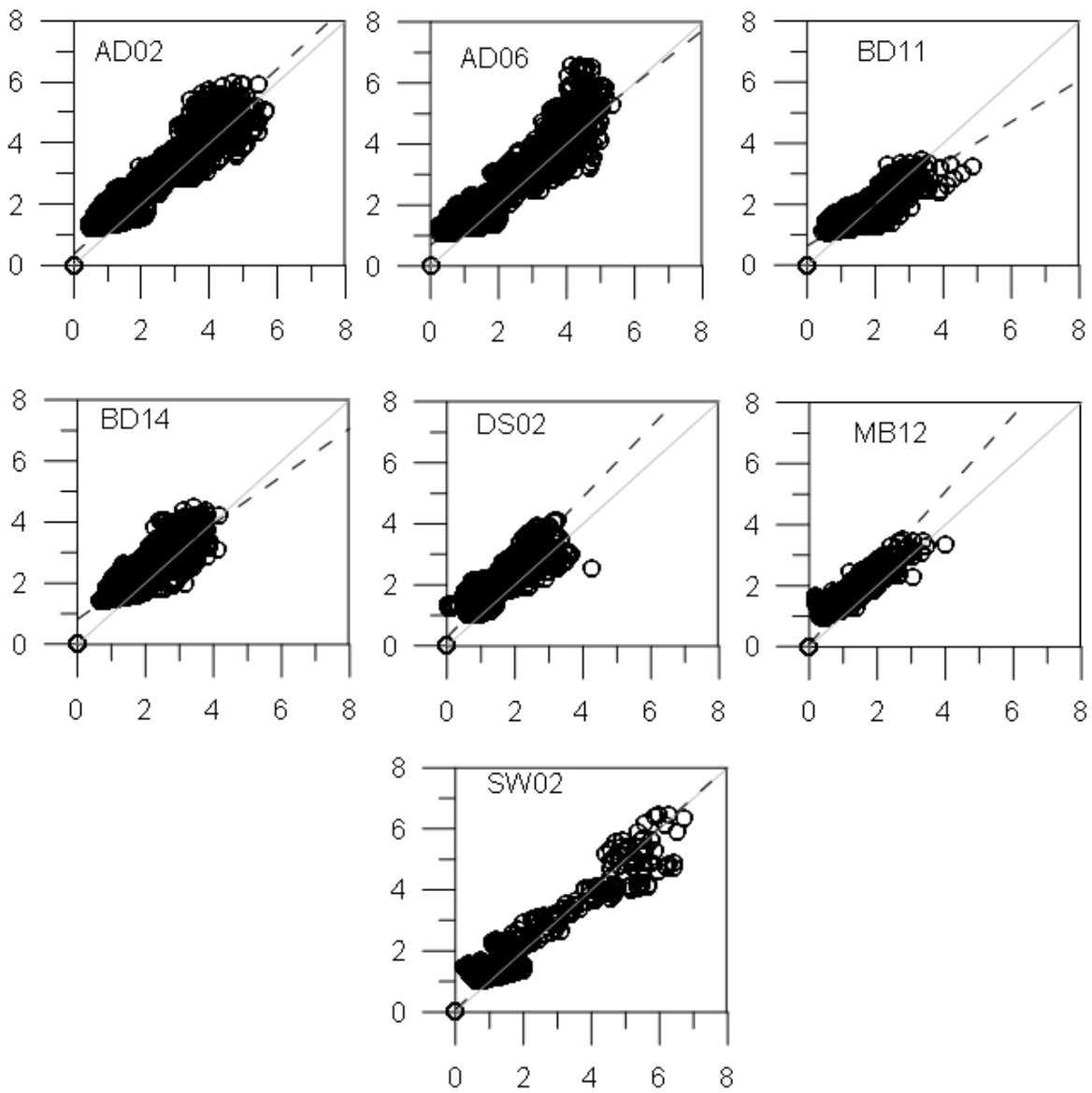


Fig. 2. Comparison plots of measured (y-axis) and modelled (x-axis) SWH for different locations in the north Indian Ocean. See text and table for details of locations and the correlation coefficients

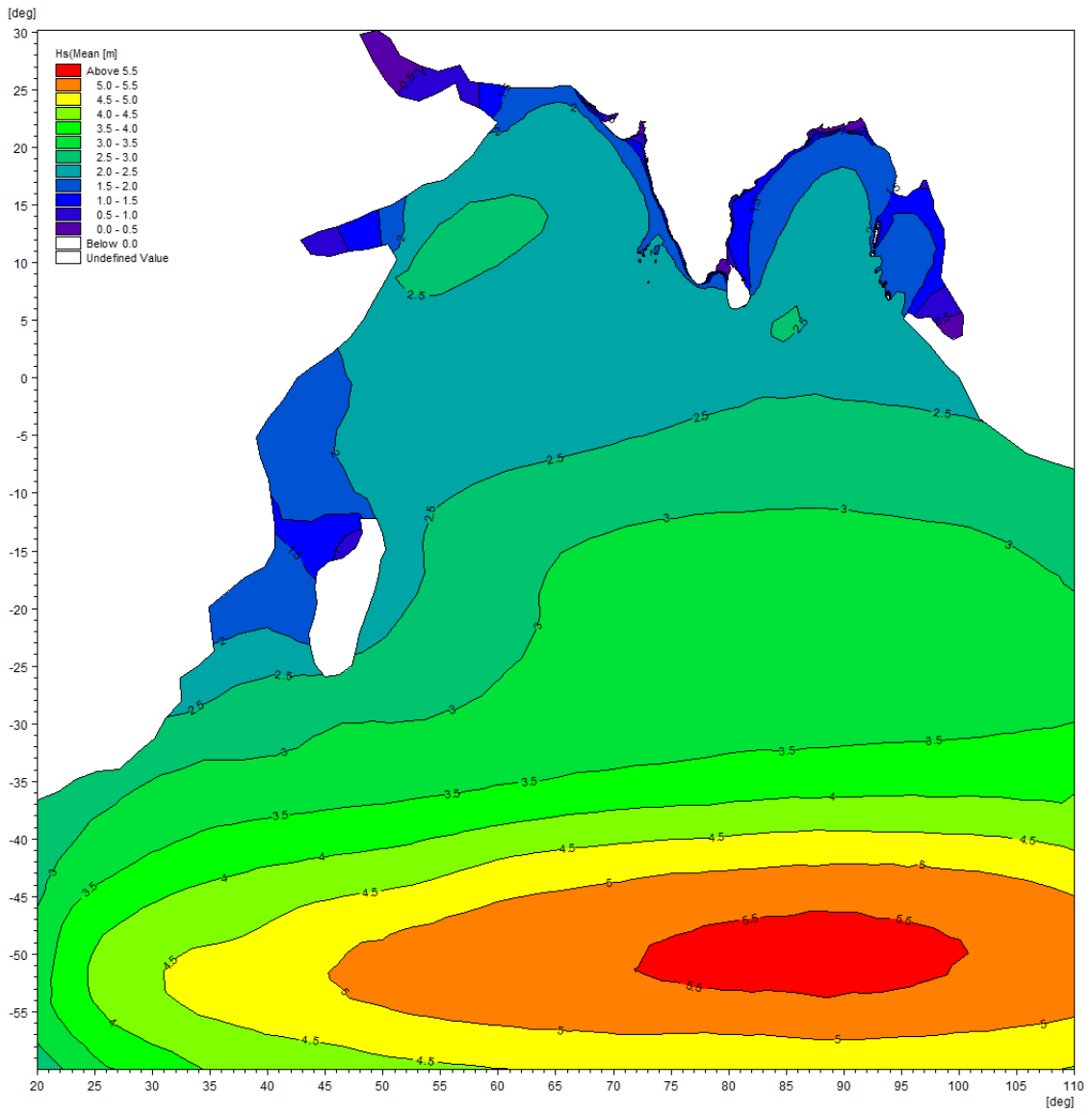


Fig. 3. Mean SWH over the 50 years

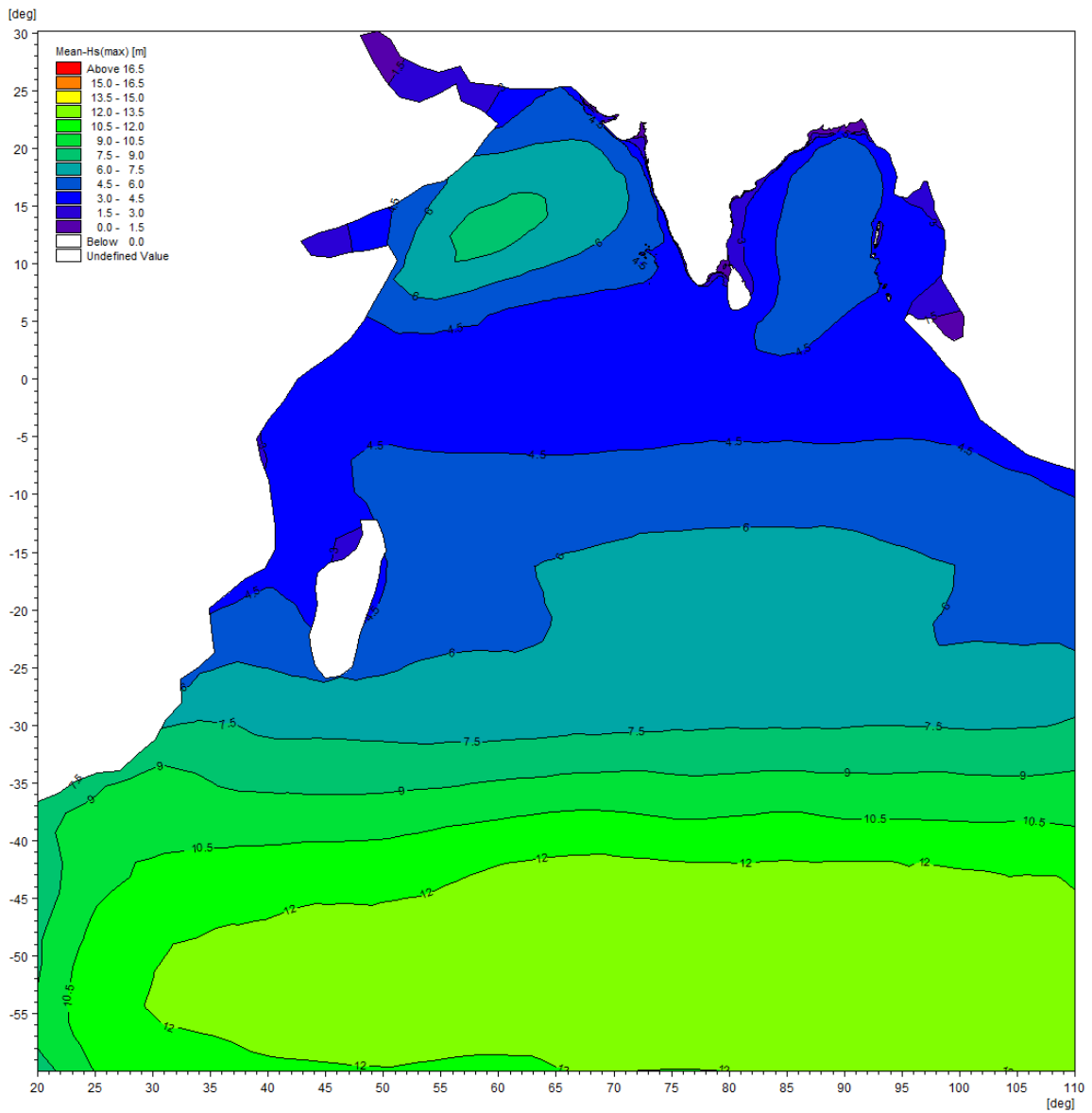


Fig. 4. Maximum SWH over the 50 years

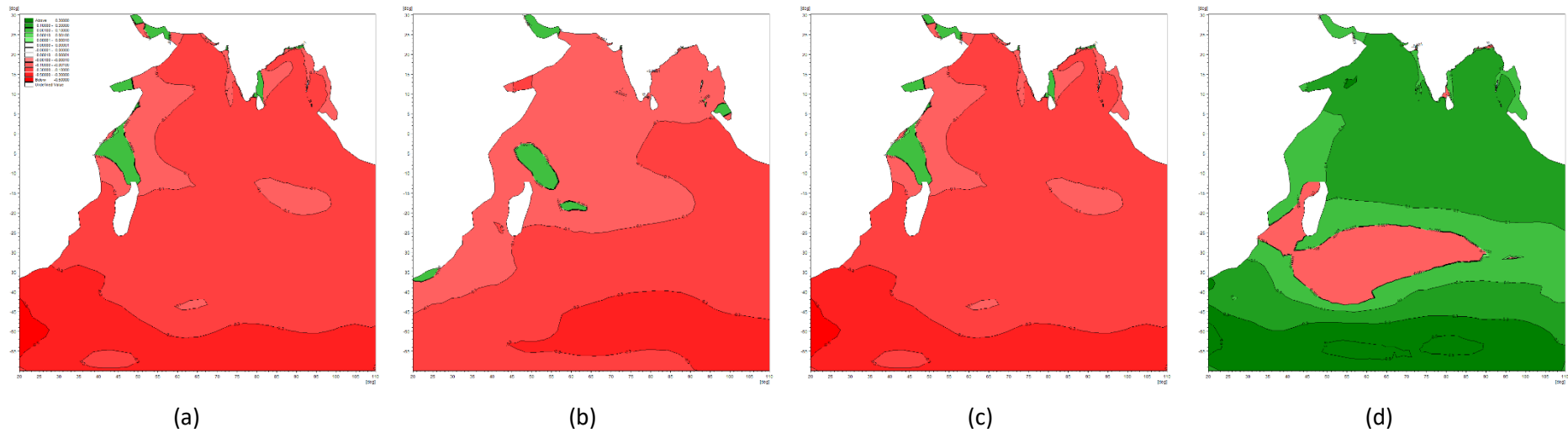


Fig. 5. Difference between the mean SWH of decades (a) D1 and D2 (b) D2 and D3 (c) D3 and D4 and (d) D4 and D5

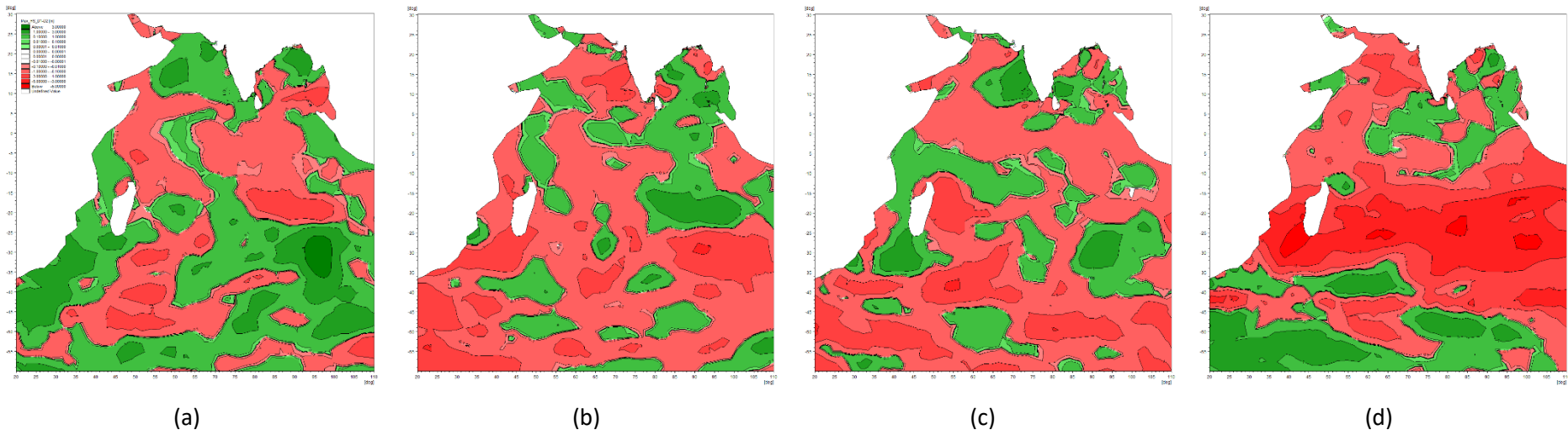


Fig. 6. Difference between the maximum SWH of decades (a) D1 and D2 (b) D2 and D3 (c) D3 and D4 and (d) D4 and D5

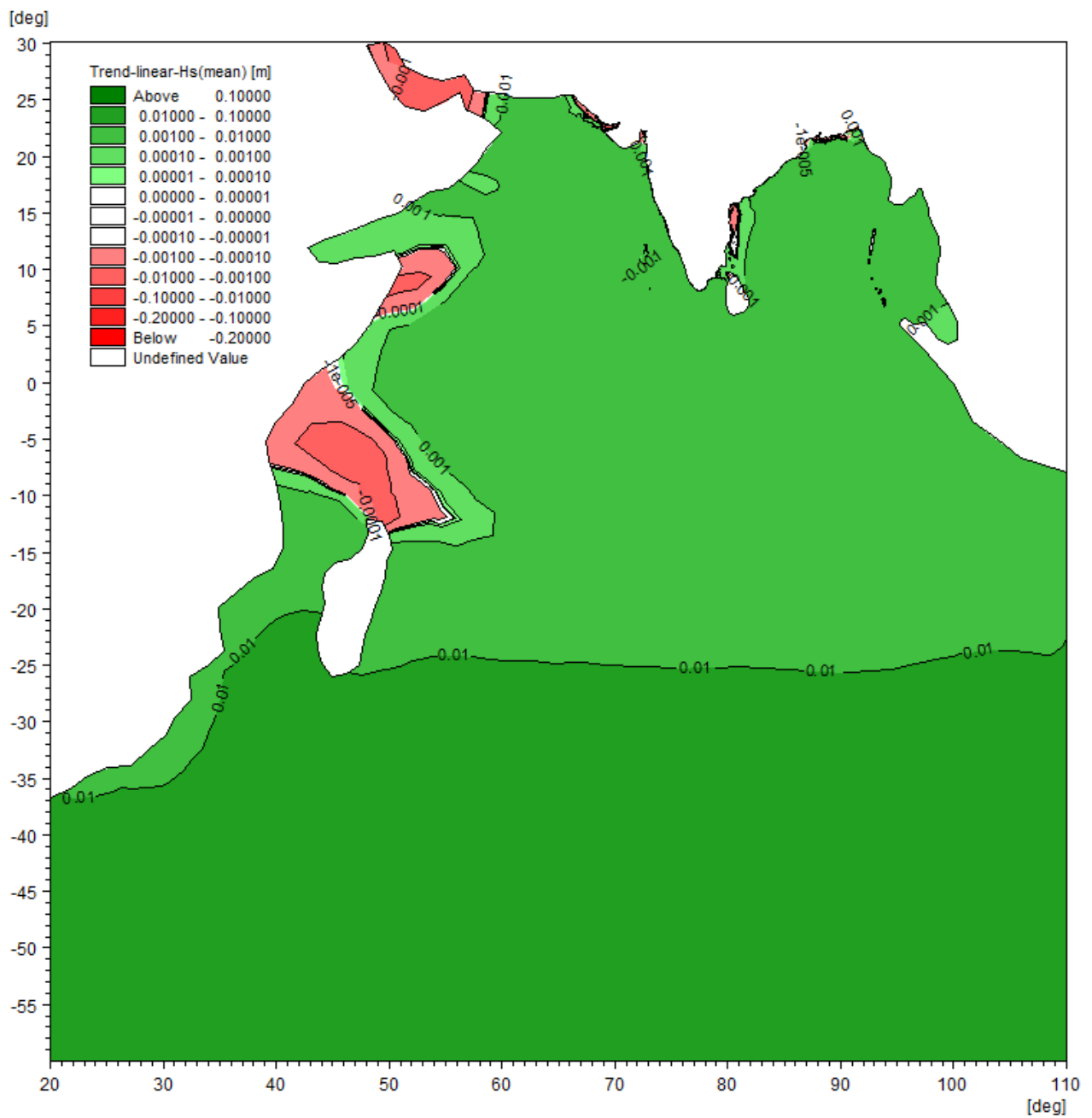


Fig. 7. Trends of Mean SWH for 50 years using linear regression

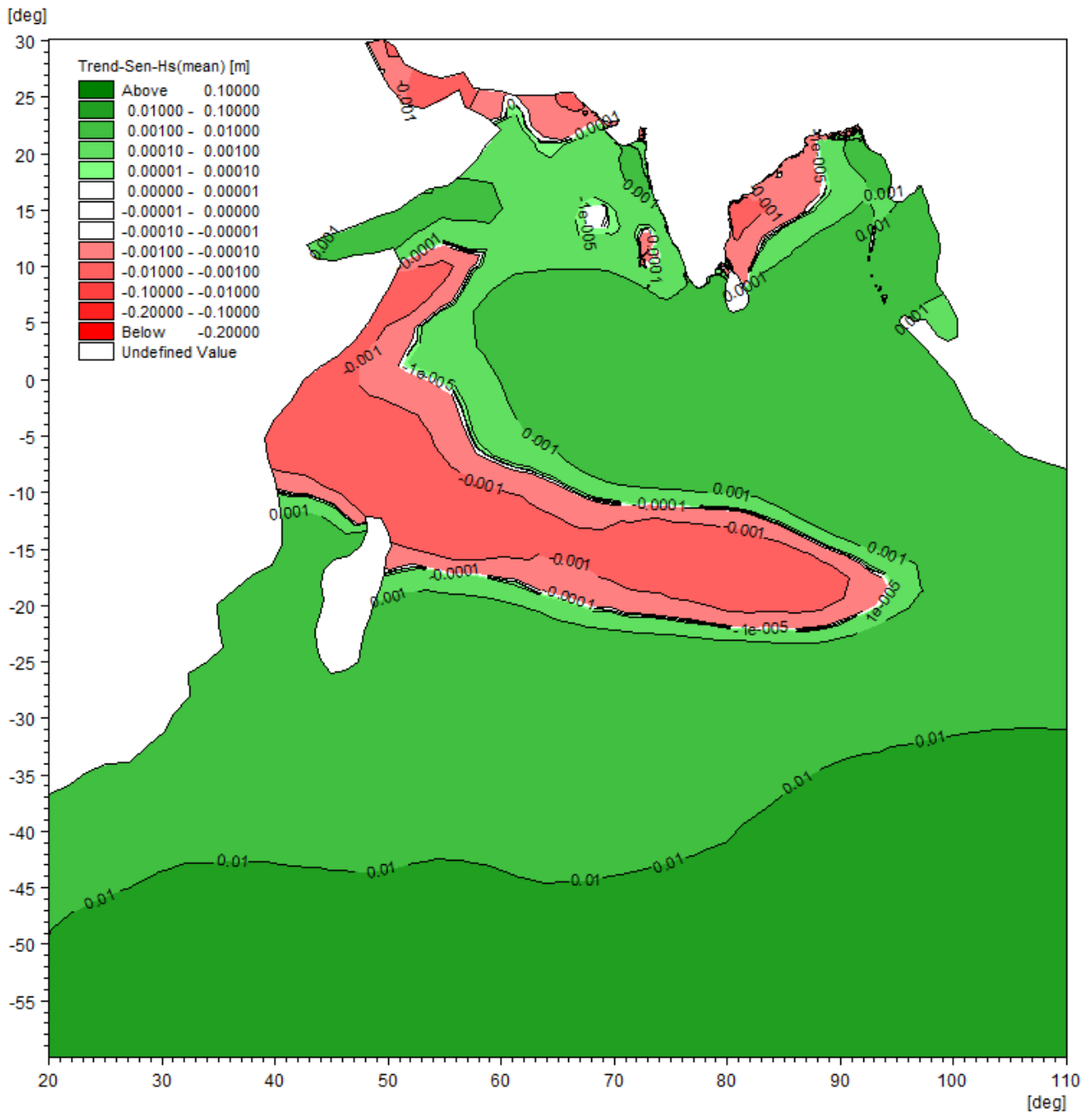


Fig. 8. Trends of Mean SWH for 50 years using Thiell-Sen's slope approach

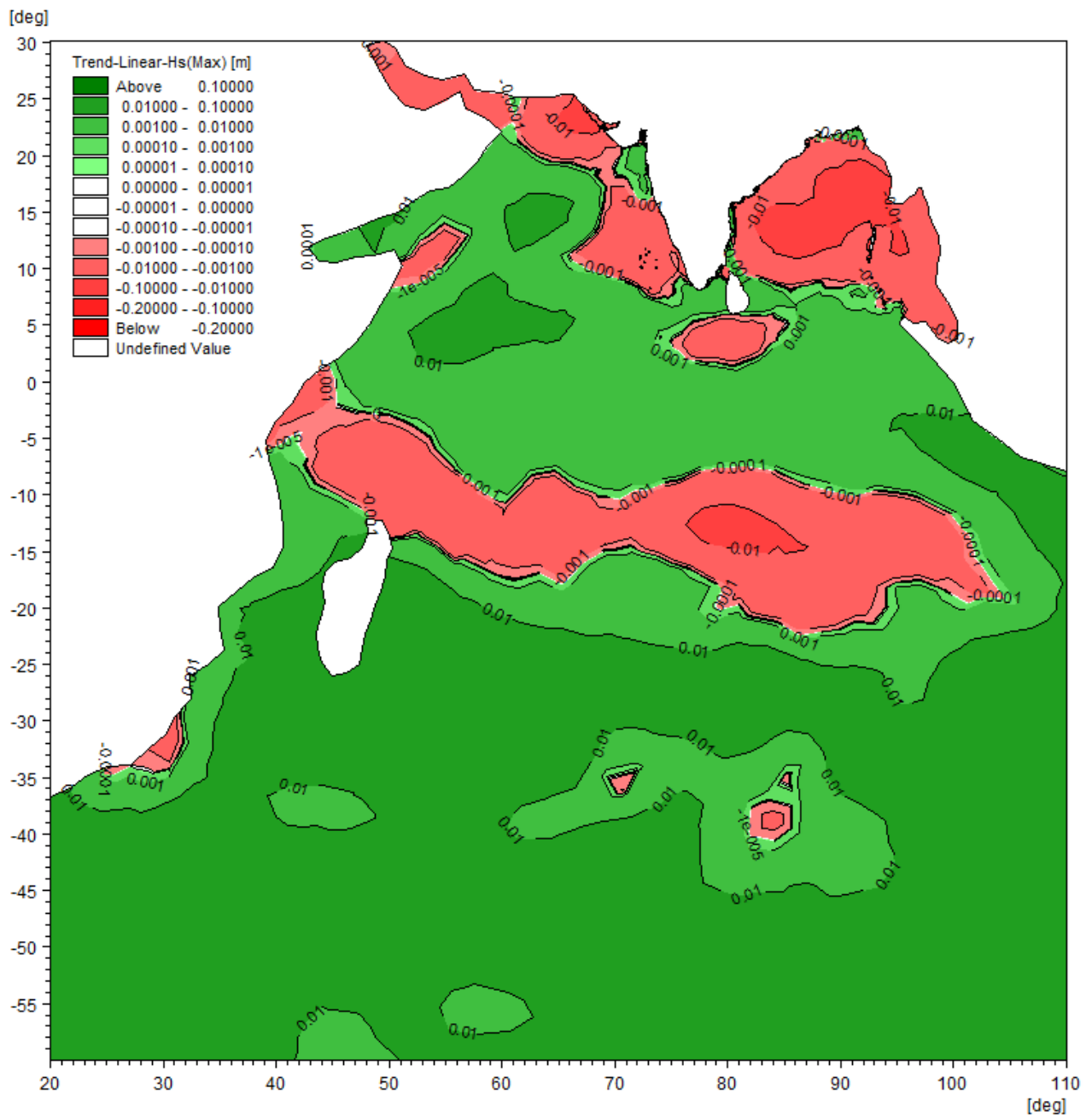


Fig. 9. Linear trends for maximum SWH for 50 years

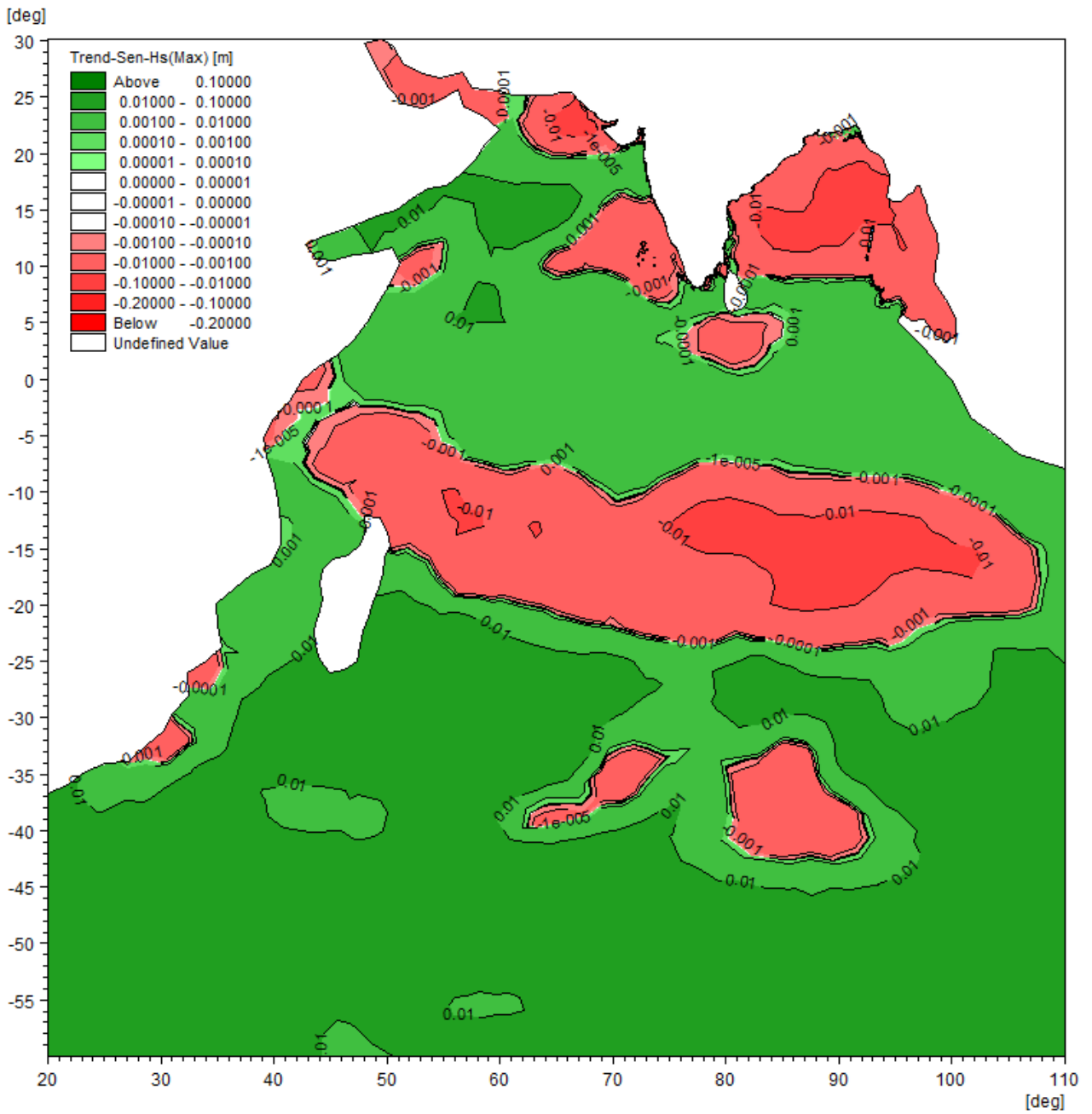
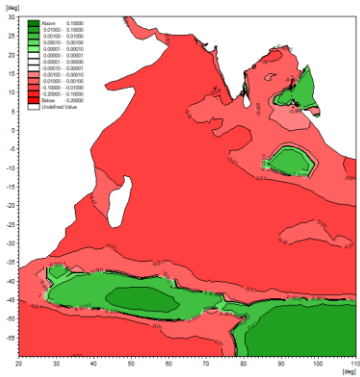
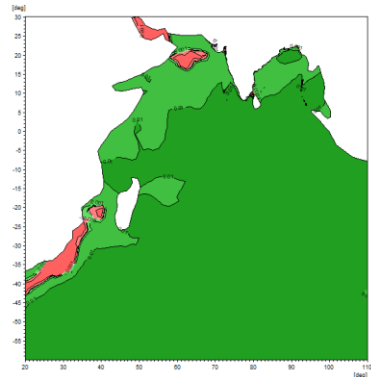


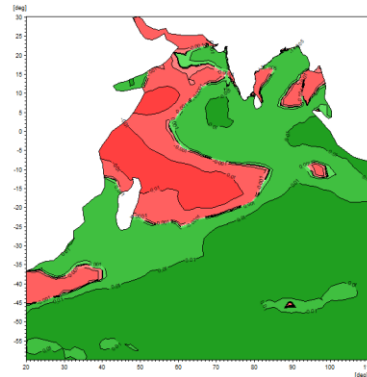
Fig. 10. Sen's slope trends for maximum SWH for 50 years



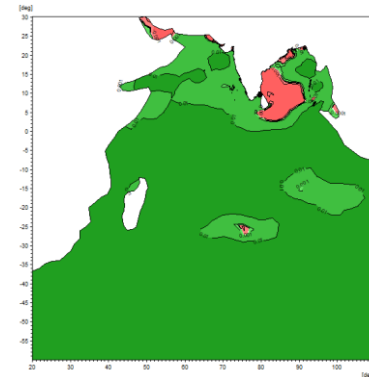
(a)



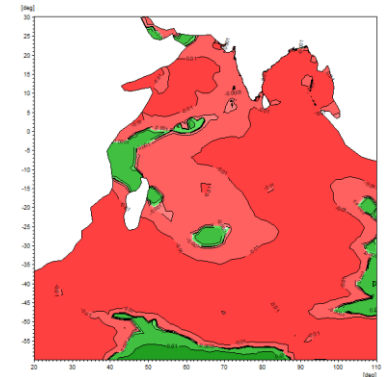
(b)



(c)



(d)



(e)

Fig. 11. Trends of mean SWH for (a) decade D1, (b) decade D2, (c) decade D3, (d) decade D4 and (e) decade D5

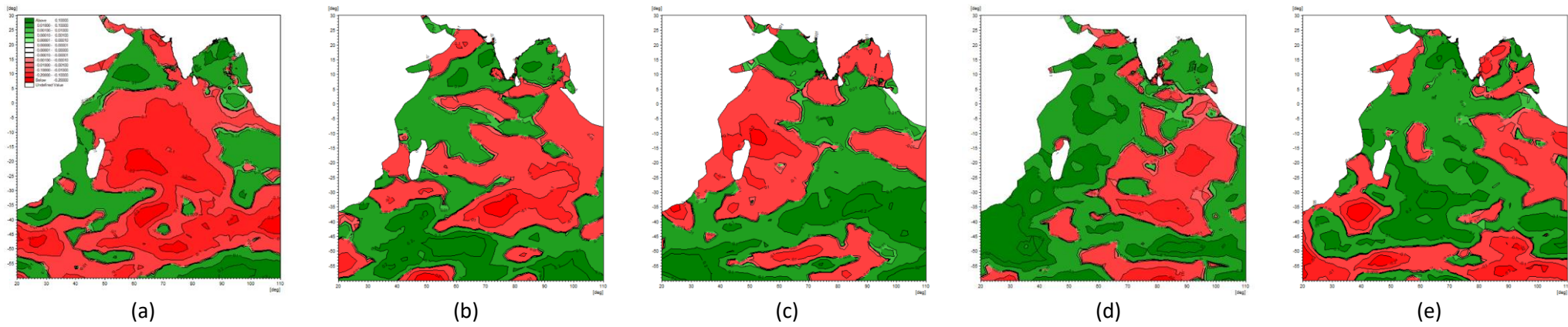
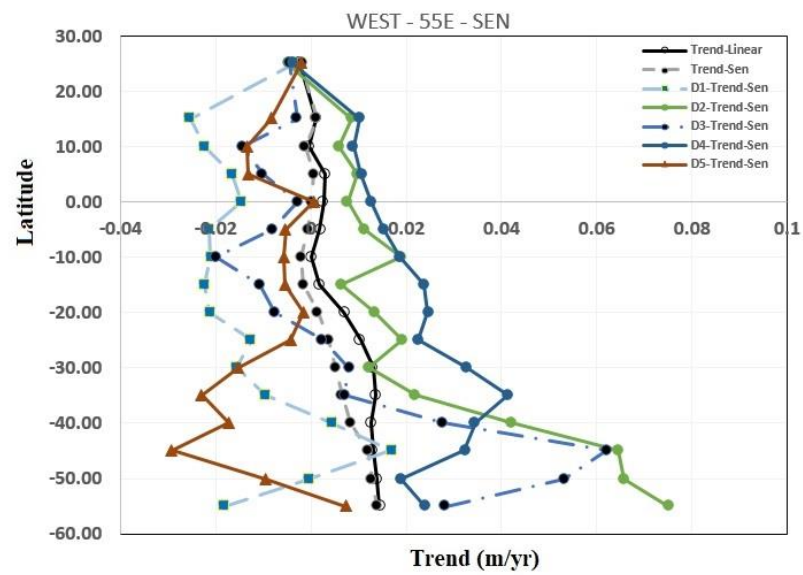
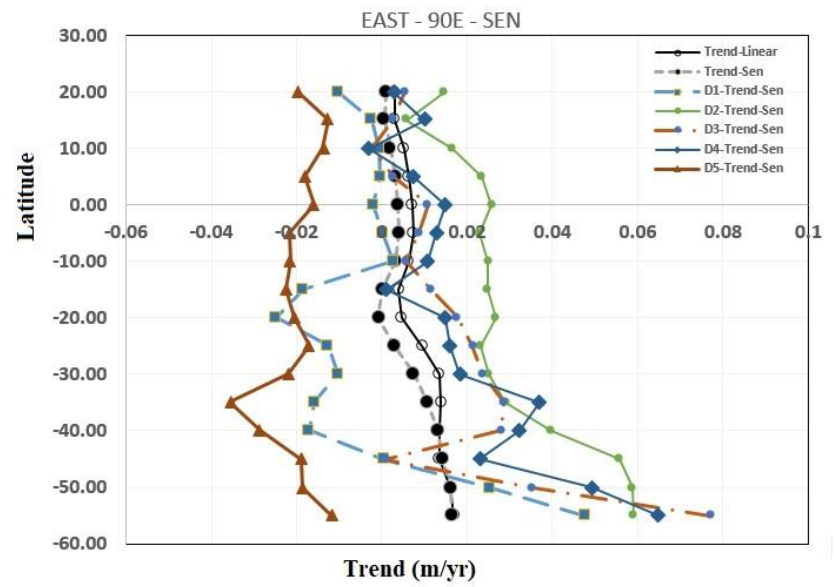


Fig. 12. Trends of maximum SWH for (a) decade D1, (b) decade D2, (c) decade D3, (d) decade D4 and (e) decade D5



(a)



(b)

Fig. 13. Mean SWH trends along (a) 55E, (b) 90E

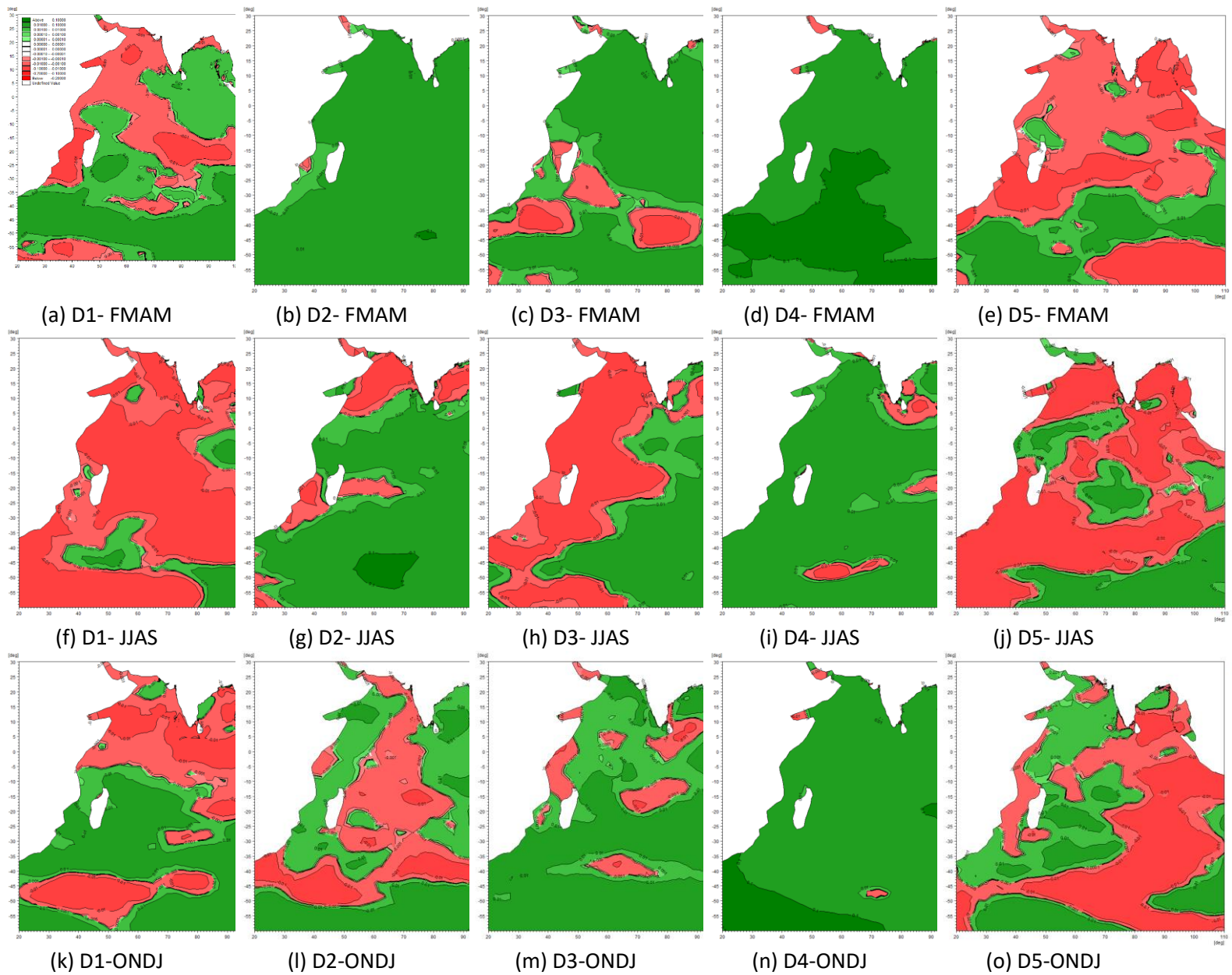


Fig. 14. Seasonal mean SWH trend SWH trend for different decades and different seasons

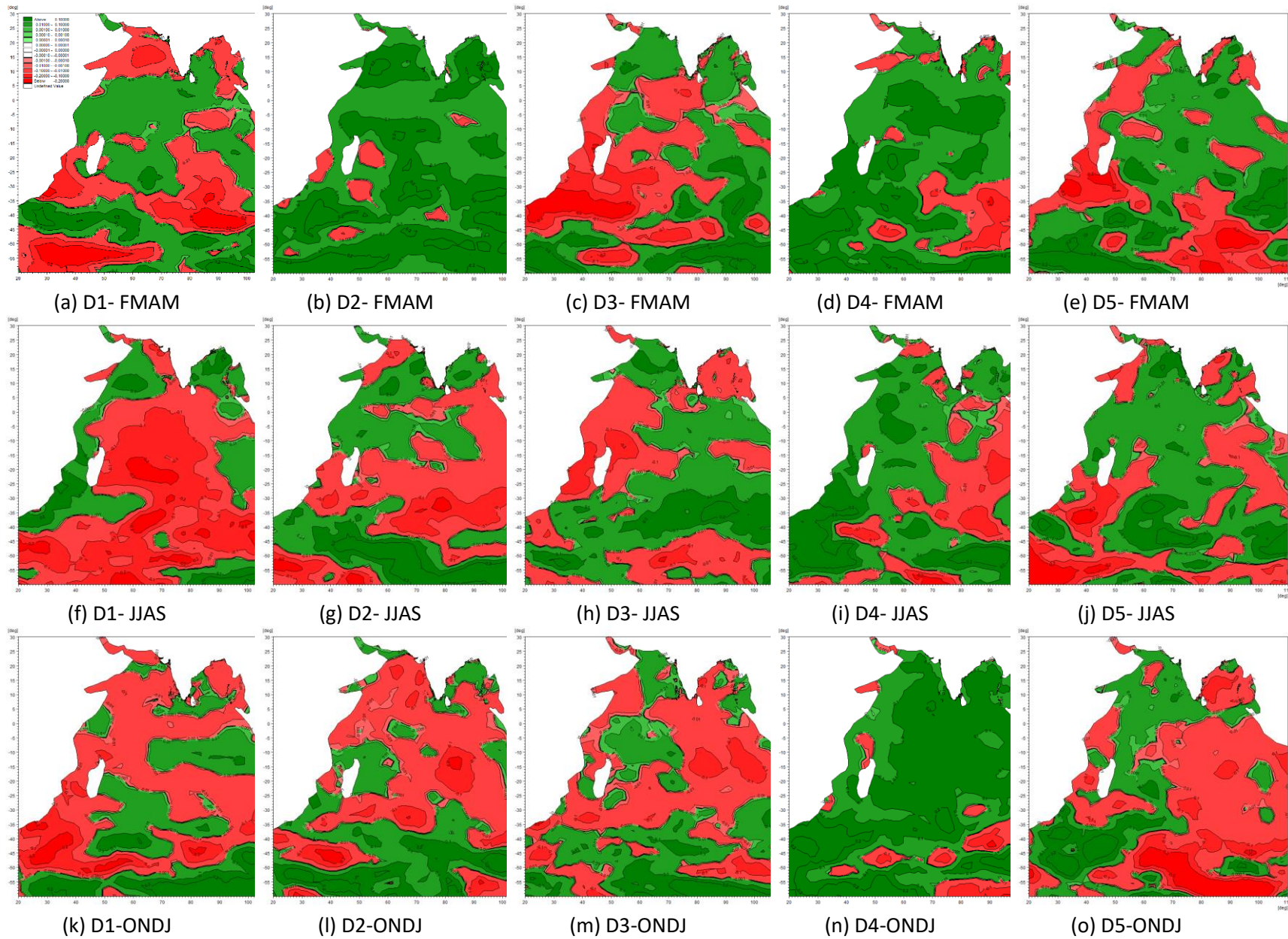


Fig. 15. Seasonal maximum SWH trend for different decades and different seasons